Constraints on the Petrogenesis of the Rockford Granite by Chemical and Radiogenic Isotopic Compositions

Robert Bishop Robbins Jr.

A thesis submitted to the Graduate Faculty of
Auburn University
in partial fulfillment of the
requirements for the Degree of
Master of Science

Auburn, Alabama
May 7, 2022

Approved by

Haibo Zou, Chair, Professor of Geosciences

David T. King, Jr., Professor of Geosciences

Mehmet Zeki Billor, Research Fellow of Geosciences

Abstract

The Rockford Granite is a Paleozoic igneous body located in Coosa County, Alabama. Regionally, between the Brevard zone and the Kowaliga zone, there lies intense faulting and shearing, which has been studied extensively relative to the tectonic relationship of the Appalachian Mountains. However, the igneous rock body that cuts across those structures has not been researched fully and its origins are not well understood. The aims of this study are (1) to characterize the Rockford Granite on the border between granite and granodiorite and (2) to further constrain the genesis and petrogenic conditions of the igneous rock body.

This thesis reports petrographic, major element, trace, and rare earth element, $^{87}Sr/^{86}Sr$ and $^{143}Nd/^{144}Nd$ compositions and biotite chemistry for the Rockford granite. Data collection of rare-earth elements on all samples has chondrite-normalized LREE-enriched patterns and flat HREE distributions. Samples 21RKF1 and 21RKF2 suggest no fractional crystallization, whereas samples 21RKF3 and 20ROCK1 display minor negative Eu anomalies, indicating moderate fractional crystallization of plagioclase. Our new radiogenic data yield initial $^{87}Sr/^{86}Sr$ ratios ranging between 0.704537-0.705938 and initial $^{143}Nd/^{144}Nd$ ratios ranging between 0.512042-0.512215. Their ε_{Nd} vs ε_{Sr} plot indicates I-type granite character and suggests that the mantle contributed not only heat but also juvenile mantle materials for the genesis of the Rockford granite. Additionally, using the AU-EMPA, biotite elemental composition data are used to determine the temperature (618-652 °C) and redox conditions (ΔQFM+1.0) for the Rockford granite.

Acknowledgments

Funding for this accelerated bachelor and master's (ABM) thesis research was provided by Dr. Haibo Zou's mass spectrometer lab recharge service account. My undergraduate research training was funded partially by the American Chemical Society Petroleum Research Fund (57500-UR2 to Dr. Zou and Dr. King). Thanks are owed to the scientists at National Petrographic Service for the diligence in preparation of the thin sections used in this research. Recognition to the scientists at Sample Solution Analytical Technology for their precise work with whole and trace element chemical analyses used throughout this research. I am indebted to my advisor Dr. Haibo Zou for providing wisdom, funding, materials, knowledge, measurements, and thesis writing advice throughout my education. This research was also greatly aided by the instruction and aid from Dr. Willis Hames in the Auburn University Electron Microprobe Analyzer (AU-EMPA) Lab and Sara Speetjens Gilley for helping in sample preparation and analyses. This research also benefitted greatly from suggestions from committee members Dr. David T King Jr. and Dr. Mehmet Zeki Billor.

Table of Contents

List of Tables

List of Figures

Introduction

Rockford Granite, located in Coosa County within central Alabama, represents an important suite of Paleozoic granitic rocks in Alabama. The generation, magmatic processes, and tectonic relationship of Alabama granitic rocks are still poorly understood. Two geochemically distinct suites of Paleozoic magmatic rocks are described in Alabama; mafic to felsic magmas known as "low-Sr/Y magmas," and a less common, "high-Sr/Y magma" (Stowell et al., 2019). Rockford has been described by Stowell as Low-Sr/Y and groups it together with the Bluff Springs Granite. Stowell et al (2019) describes Low-Sr/Y granites to appear to be S-type granites rich in aluminum. Previous research, within the state of Alabama along the Eastern Blue Ridge of the southern Appalachian orogen, has presented geochemical analysis of the varying igneous rocks. Zircon U-Pb, and Sr isotope analysis has been calculated, but these previously reported $^{87}Sr/^{86}Sr$ values have large uncertainties (Russell et al., 1989).

This work will further investigate and update the work done by others such as Russell et al (1978), Foord et al (1989), and Stowell et al (2019). Russell's work primarily focused on Sr isotopes from the broader Appalachian orogen within Alabama and the Sr isotope data can now be much more precise. Two years later, Foord (1989) expanded upon the work done and presented a more detailed report of the Rockford Granite and its chemical composition. Recent work completed by Stowell et al (2019) has since updated the ages using U-Pb and gathered "representative compositions" of the Rockford Granite. Whereas all this work builds upon each other, none of the past researchers have focused on Rockford and provided a detailed analysis for this specific unit. Neodymium isotope data critically for evaluating granite petrogenesis are lacking for Rockford Granite.

Objectives

The primary focus in the proposed research will be to further investigate the petrogenesis of the Rockford Granite, for example, the characteristics of the source rocks, and the roles of crust and mantle contributions. Notable information can be derived from radiogenic isotopic signatures regarding the source and evolution of granitic rocks that cannot be determined by prior research methods. Specifically, rubidium (Rb)-strontium (Sr) isotope systematics and samarium (Sm)-neodymium (Nd) isotope systematics to determine the sources and magmatic processes for the Rockford Granite. Further analysis into mineral compositions will provide constraints on the crystallization conditions (temperature and redox conditions) of the Rockford Granite. Combining isotope and chemical analysis with petrographic work will provide new insights into the formation of the granite, while simultaneously updating and further refining work accomplished by others.

This research aims to answer the following: What are the source rocks for the Rockford granite? Is the magma that formed the Rockford granite primarily crustal, or mantle derived? What is the role of mantle for the formation of the Rockford granites? Under what conditions did the granite form?

Background

Geologic Setting

Alabama granites of this research lie along the Brevard fault zone, south of the Appalachian Mountain range. Earlier studies have noted that the Brevard zone has a “locus of intense shearing and faulting” (Rankin, 1975). Scientists describe the region as a shear zone approximately 356 million years ago, however most dikes cut across it undisturbed, suggesting that the zone was no longer active at the time of igneous intrusions.

Outside the Brevard zone lies the Alabama Piedmont, a large region that can be divided into three lithotectonic provinces: the Northern Piedmont, Inner Piedmont, and Southern Piedmont. Within the Inner Piedmont, between the Brevard zone and the Kowaliga zone, lies the locations for our sample collection. Varying lithologies occur in the Inner Piedmont such as: hornblende schists, amphibolites, gneisses, aluminous meta-pelites, biotite gneisses, mica schists, and quartzites (Stow, 1984). Most lithologies are intruded by granite plutons, which are the focus of this paper. Noted by Stow et al. (1984) the igneous activity predated the major prograde regional metamorphic event that raised rocks to the Barrovian amphibolite facies. The Rockford Granite is, as shown in Figure 1, part of the middle-to-upper-amphibolite facies Wedowee and upper-amphibolite facies Hatchet Creek Groups (Drummond, 1988).

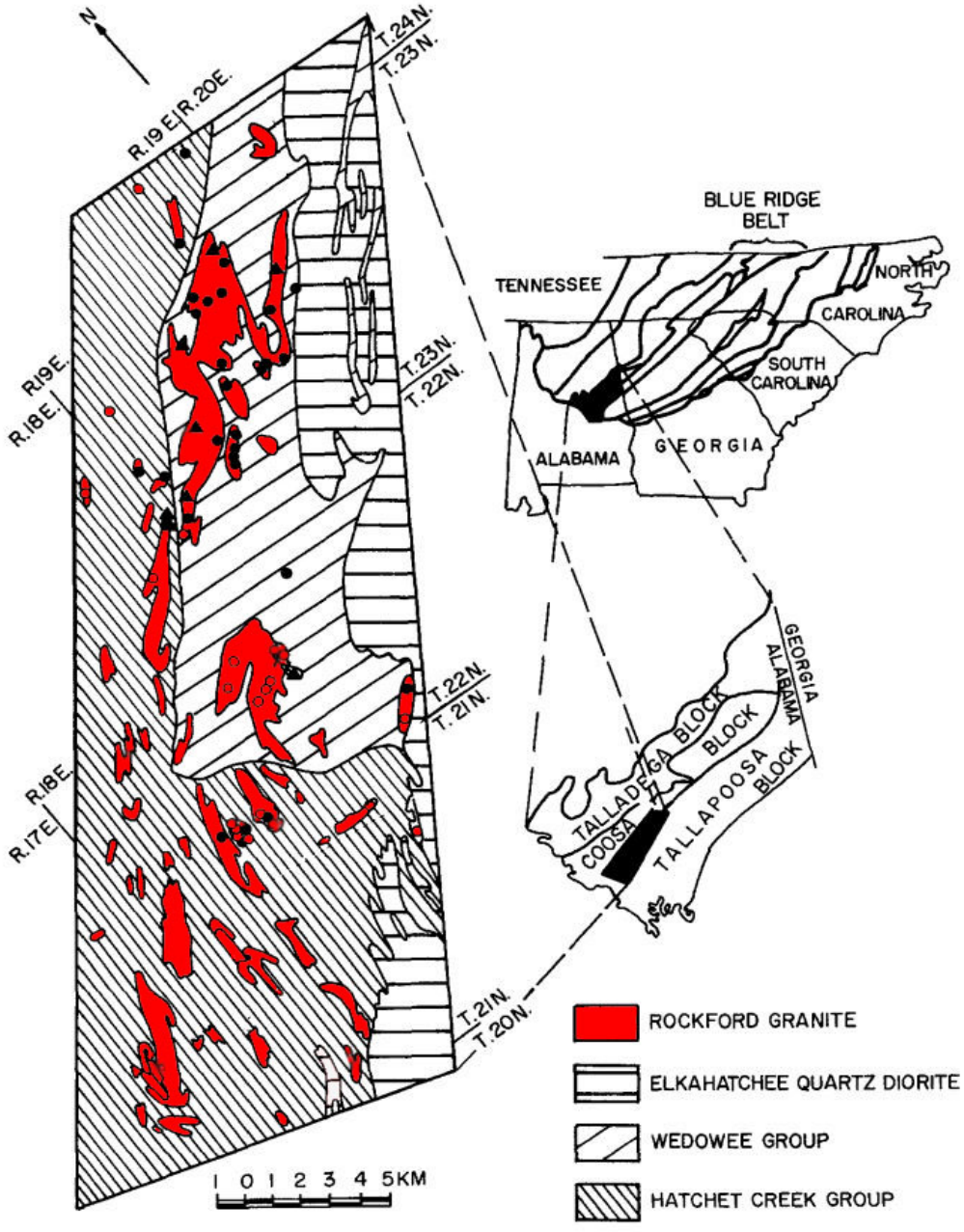

Figure 1- Modified regional map providing context for the geologic location relative to the surrounding groups (Drummond, 1986; 1988)

Concerning Samarium-Neodymium Isotope Systematics

Within the Lanthanide series, the elemental parent Samarium (Sm)-147 decays to Neodymium (Nd)-143 via alpha decay with a half-life of 106 billion years. Although alkaline igneous rocks have higher Sm-Nd ratios than calc-alkaline, all igneous rocks have some relationship between these two elements allowing for simple constraints on the rock being analyzed. This is aided by both elements being even numbered in the Lanthanide series with similar chemical and fractionation properties. Neodymium is more incompatible than Sm, which means it favors the melt; this causes melts to have a low Sm/Nd ratio while any residue will have a high Sm/Nd ratio. The model age, described as T_{CHUR}, describes the formation of the rock from the chondritic uniform reservoir (CHUR) which provides crustal formation age and is used in this research. Sm-Nd isotope systematics are not affected by pressure or temperature conditions, instead their ratio reflect source characteristics.

Plotting Sm-Nd systematics as ε_{Nd} vs ε_{Sr} allows us to constrain the source rock and classify it as such. Rb-Sr isotopes are explained in the next section, however, we plot ε_{Nd} and ε_{Sr} because each isotope system has an element that is incompatible and prefers the melt: Nd and Rb respectively. Calculations performed are from the formula shown below, where $^{143}Nd/^{144}Nd$ CHUR value of 0.512638 is used.

$$\varepsilon_{Nd} = \left[\frac{\left(\frac{^{143}Nd}{^{144}Nd}\right)_{sample} - \left(\frac{^{143}Nd}{^{144}Nd}\right)_{CHUR}}{\left(\frac{^{143}Nd}{^{144}Nd}\right)_{CHUR}} \right] \times 10000$$

Concerning Rubidium-Strontium Isotope Systematics

Within the alkaline metals is rubidium (Rb), while strontium (Sr) lies within the alkaline earth metals, both elements provide geochemical information about igneous rocks and their processes regarding their formation. Strontium is one of the most abundant trace elements on earth, making it readily available for analysis. Calcium and strontium have a similar ionic radius and same charge (+2) which allows easy substitution of Sr in the mineralogical structure of various minerals hosted within the igneous rock. Rubidium-87 undergoes beta minus decay to the stable ^{87}Sr, allowing the ratio of Rb/Sr to be utilized as a tool to understand geochemical conditions for formation. Rubidium is also useful when comparing the two elemental isotope pairs because Rb is more incompatible and thus will prefer melts. However, this work primarily utilizes the Sr isotope systematics. Unlike other major and trace element concentrations, $^{87}Sr/^{86}Sr$ ratio is ideal for constraining petrogenesis because it is not affected by processes such as partial melting and closed-system fractional crystallization. This property makes Sr isotopes a useful tool for petrogenesis analysis.

Natural Sr consists of four stable isotopes: ^{84}Sr; ^{86}Sr; ^{87}Sr; and ^{88}Sr (Faure and Mensing, 2005). Abundance varies due to radiogenic ^{87}Sr production. ^{87}Sr is produced through beta decay of ^{87}Rb, which has a half-life of approximately 49 billion years. The Rb-Sr system is an extremely useful isotopic parent-daughter system for both age dating and petrogenetic studies. When analyzing Sr,it is common to use the ratio of $^{87}Sr/^{86}Sr$, because ^{86}Sr is a stable isotope and is not created as a product of the breakdown of any other element.

Materials and Methods

Sample Preparation

Samples collected in Coosa County were all found in place and were then broken off and removed of any weathering surface features that may have been present. Collected samples were from the northern, southern, and western ranges of the Rockford Granite allowing a wide range of potential chemical changes.

For multi-collector inductively coupled plasma mass spectrometer (MC-ICP-MS) analyses, electron microprobe analyses, and petrographic analyses, the samples required smaller and even fresher cores. This was accomplished using a rock saw in Auburn University's sample preparation lab. After samples were cut, they were sent to National Petrographic for polished thin section preparation as well as to Sample Solution Analytical Tech for $^{143}Nd/^{144}Nd$ and $^{87}Sr/^{86}Sr$ isotope analyses. For Sm-Nd and Rb-Sr concentration data, a single collector (ICP-MS) was used.

$^{87}Sr/^{86}Sr$ and $^{143}Nd/^{144}Nd$ isotope data collection

Sr and Nd isotopic compositions were analyzed by Neptune Plus MC-ICP Mass spectrometer (Thermo Fisher Scientific, Dreieich, Germany) in the Sample Solution Analytical Tech. Analytical methods have been documented in Li et al. (2012).

Electron Microprobe

Four polished thin sections were made by National Petrographic Service. Samples 21RKF1 and sample 21RKF3 were chosen due to their textural and mineralogical differences determined by visual and microscopic analysis. Operating conditions of the microprobe were as follows: accelerating voltage = 15kV, beam current = 20nA, beam size = 1 μm. Calculations were performed using the ZAF matrix correction (Z: atomic number; A: absorption effect; F: fluorescence effect) correction program supplied by JEOL corporation.

Preparation for the thin section analysis required the two samples to be placed in a carbon vacuum evaporator which coats the samples in carbon from graphite. Carbon on the surface of the thin sections creates an electrically conductive surface and prevents the accumulation of charge while under the electron microprobe. Samples were then input into the Auburn University Electron Microprobe Analyzer (AU-EMPA), shown in Figure 2. The AU-EMPA, model JEOL JXA-8600, was standardized to biotite and garnet. Point analyses were performed on several mineral grains in both samples in various locations throughout the thin section to prevent analyses near each other.

Figure 2- Auburn University Electron Microprobe Analyzer (AU-EMPA).

RESULTS

Optical Petrography

Sample 21RKF1 is primarily composed of quartz, biotite, and plagioclase. Quartz grains contribute ~30% of the total rock and are very fine and range in size from 1-3mm. Biotite grains contribute ~40% of total composition and are roughly 1-3 mm in size with no apparent foliation. Plagioclase grains provide the remaining ~30% of the total rock and average 4mm in size and are randomly oriented.

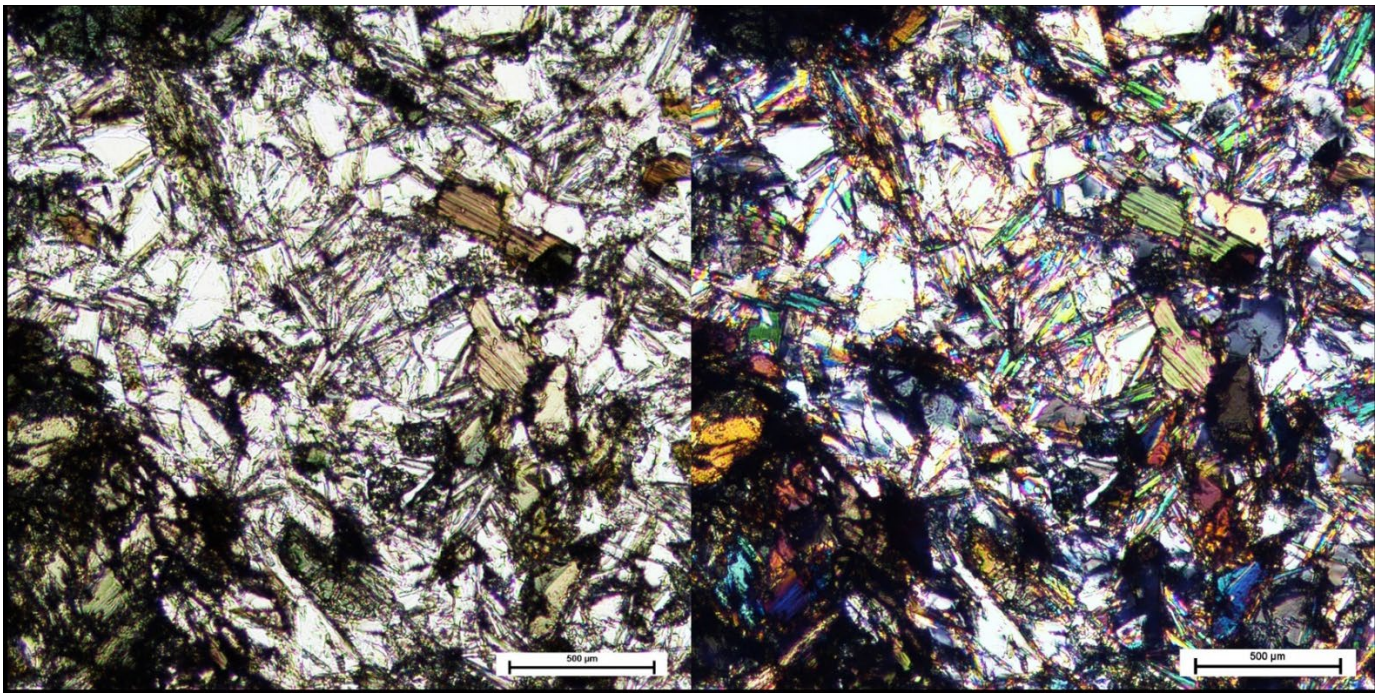

Figure 3 – Petrographic images of sample 21RKF1. On the left, in plane polarized light (ppl), and on the right, cross-polarized light (cpl).

Sample 21RKF2 is composed primarily of quartz, biotite, and plagioclase. Quartz grains vary in color from white, with no discernible size, to light gray grains averaging 3-4mm. Biotite is much less present in 21RKF2 and averages 1-2mm in size. Plagioclase grains appear to generally follow the same orientation across the whole rock and are either ~4mm or ~1mm in

length. Compositionally, quartz makes up ~40% of the whole rock, with biotite ~20%, 25% plagioclase, and 10% potassium feldspar with very minor muscovite.

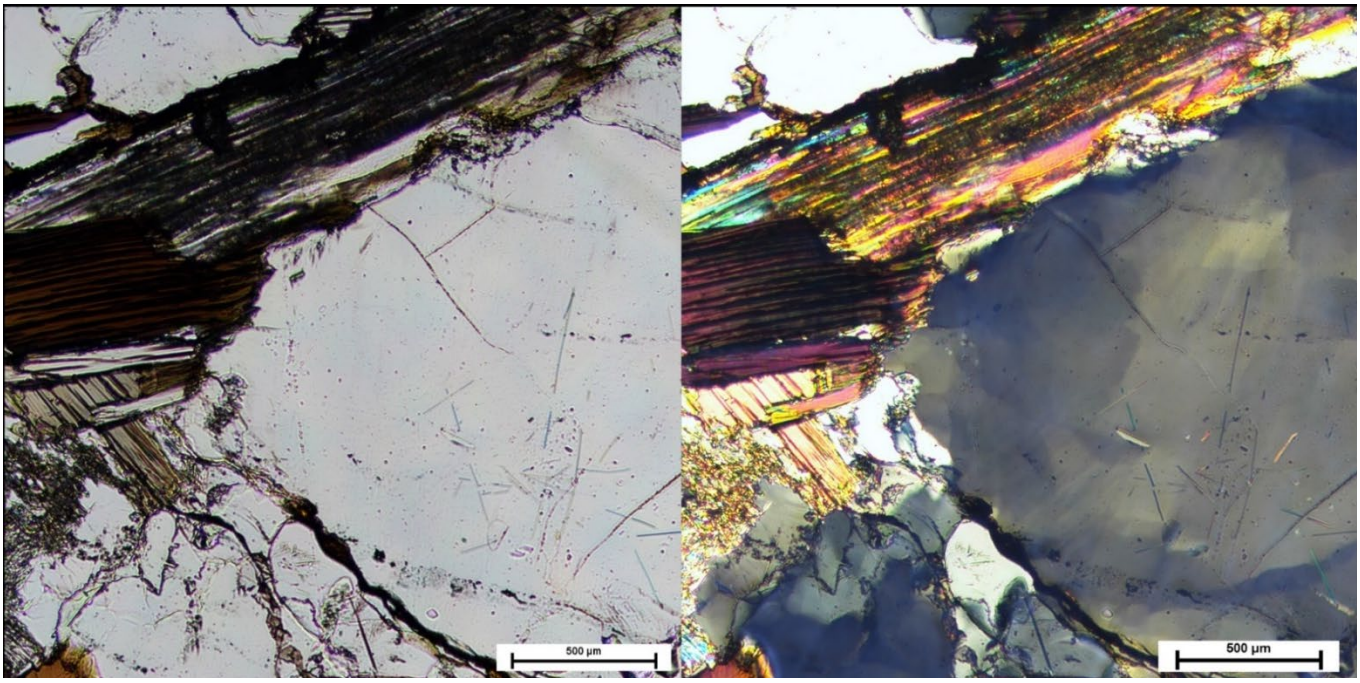

Figure 4- Petrographic images of sample 21RKF2 on the left in ppl and on the right cpl.

Sample 21RKF3 is composed of quartz, biotite, muscovite, and plagioclase. Quartz grains vary in color from white, with no discernible size, to light gray grains averaging 2-3 millimeters. Biotite grains appear to be more clustered together in 21RKF3 but still remain around 1-2mm in size. Plagioclase grains also appear to generally follow the same orientation and are consistently around 1-2mm. Muscovite appears more commonly in 21RKF3, however grains are less than 1mm in length and appear around the outer edge of plagioclase grains. Compositionally, quartz makes up ~40% of the whole rock, with ~25% biotite, 15% plagioclase, 10% potassium feldspar,

and subordinate muscovite.

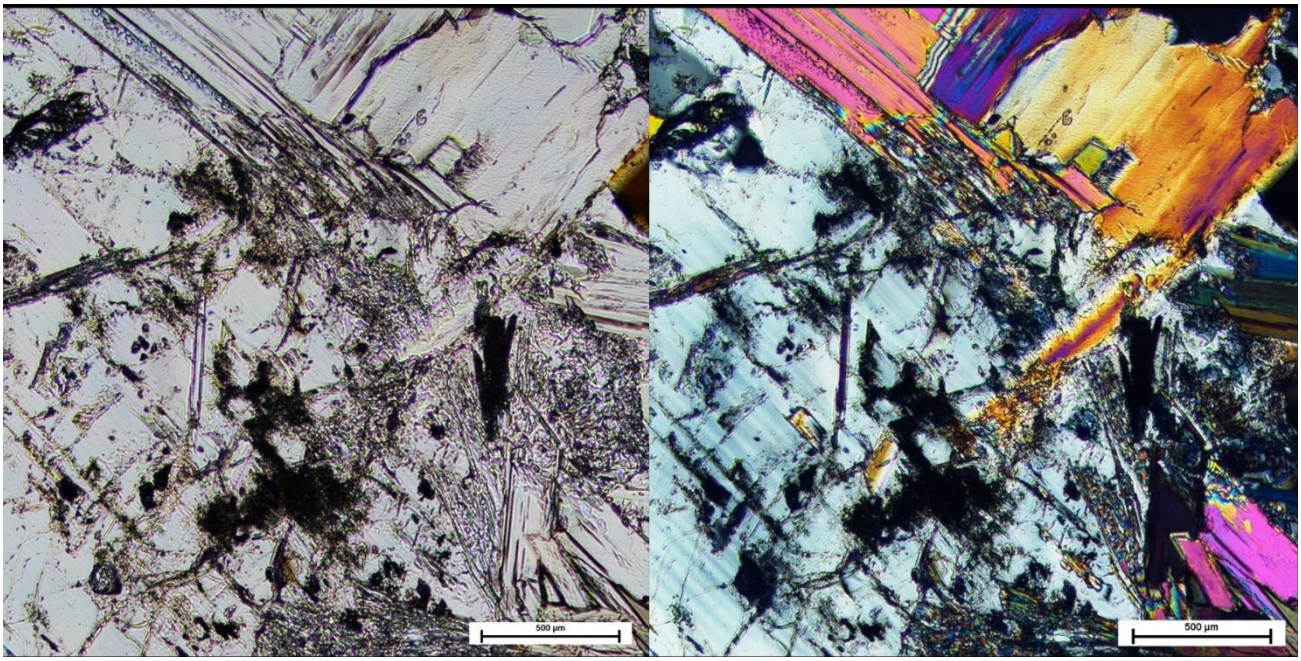

Figure 5- Petrographic images of sample 21RKF3 on the left in ppl and on the right cpl.

Sample 20ROCK01 is similarly primarily quartz, biotite, muscovite, and plagioclase. Quartz grains vary in color from white, with no discernible size, to light gray grains averaging 2-3mm. Sample 20ROCK1 appears to have much more light gray quartz grains than white. Biotite grains appear more randomly throughout but still remain around 1-2mm. Plagioclase do not appear to follow any orientation and range in size from less than 1mm to 4mm. Muscovite grains are less than 1mm to 2mm and continue to appear around the outer edges of plagioclase grains. Compositionally, quartz makes up ~40% of the whole rock, with biotite ~25%, and 25% plagioclase, 10% potassium feldspar, and subordinate muscovite.

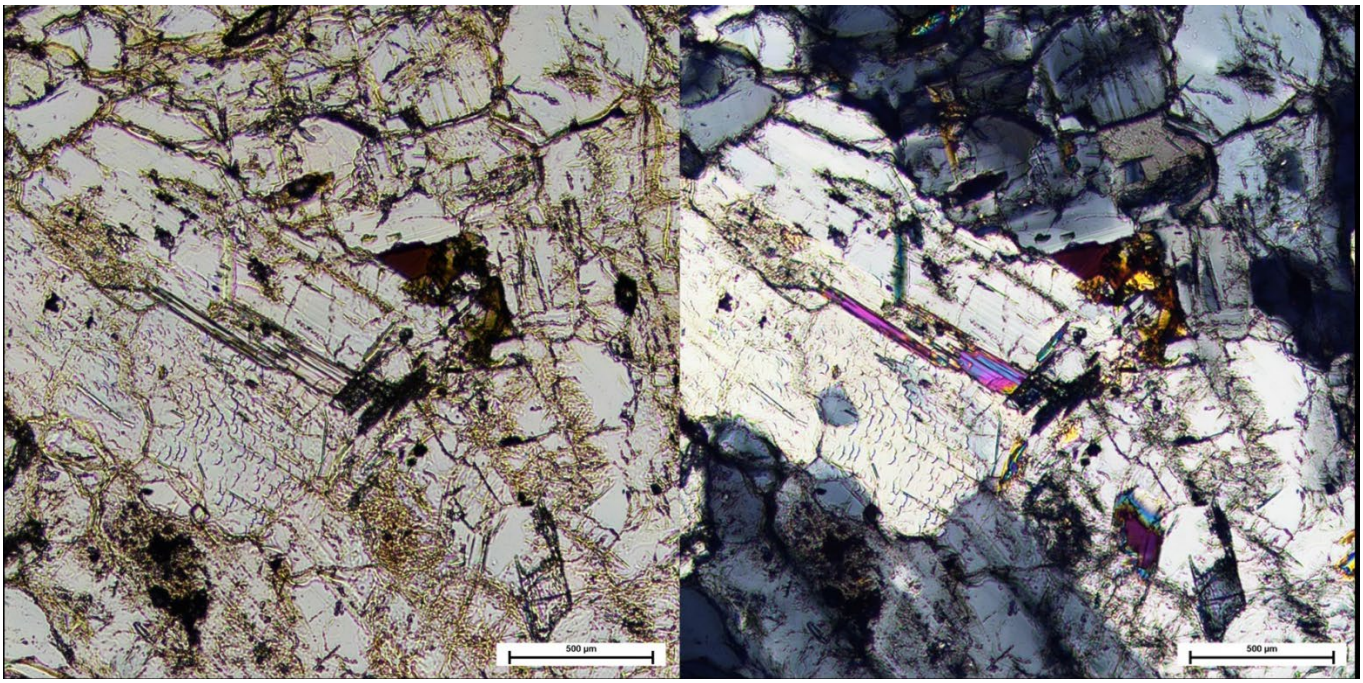

Figure 6- Petrographic images of sample 20ROCK1 on the left in ppl and on the right cpl.

Major Element Results

According to our major element data on total-alkali-silica (TAS) plot (Fig. 7), 21RKF1 is monzo-diorite, 21RKF2 and 21RKF3 are granodiorite, and 20ROCK1 is granite. In the Harker diagram, for granodiorites and granites, TiO_2, Al_2O_3, MgO, CaO, Na_2O decrease while K_2O increase with increasing SiO_2. Fe_2O_3 and MnO do not show correlations with SiO_2. The decrease of TiO_2 with increasing SiO_2 indicate fractional crystallization of Fe-Ti oxides. The decrease of Al_2O_3, CaO and Na_2O suggests fractional crystallization of plagioclase. The increase of K_2O with increasing SiO_2 argues against of fractional crystallization of K-feldspar.

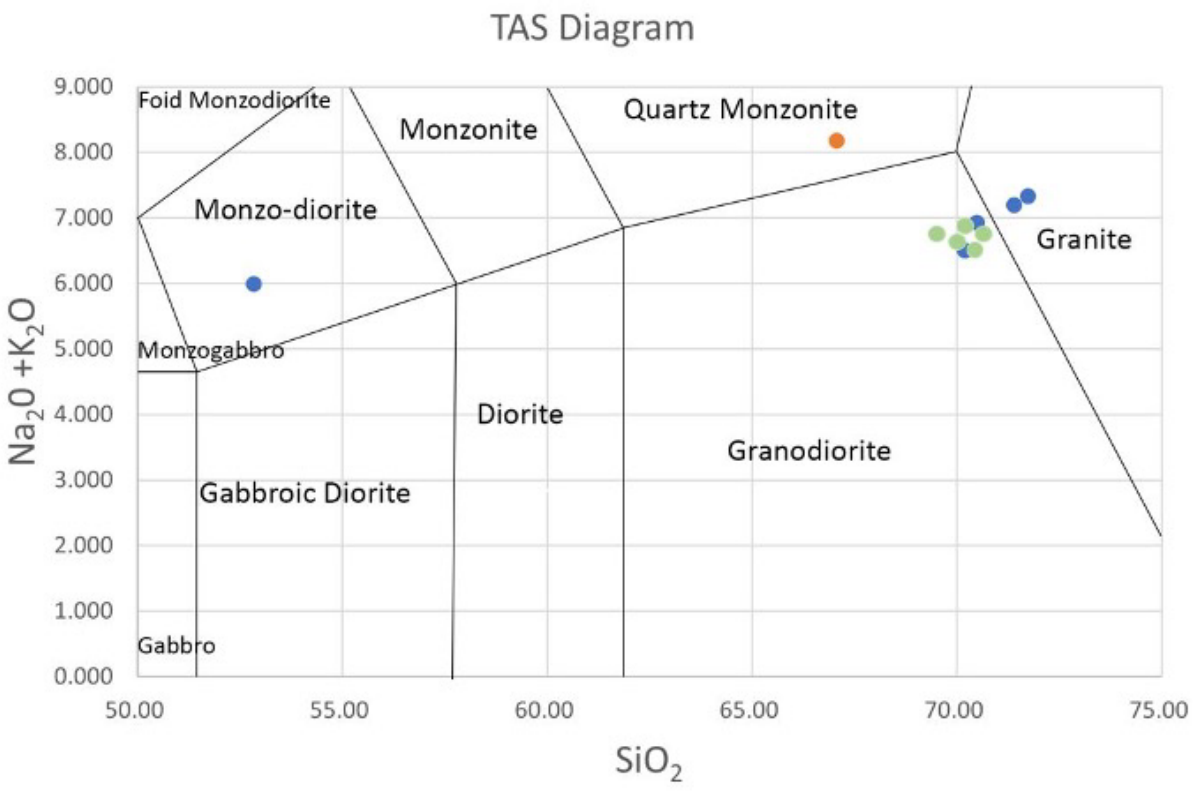

Figure 7- A TAS diagram of samples from the Rockford granite. Using Middlemost's method of naming plutonic rocks, all our new samples (blue dots) border the Granodiorite and Granite boundary except for 21RKF1, which lies in the Monzo-diorite field. Orange circle is Stowell et al's (2019) data, green circles represent Foord et al's (1989) data. See Middlemost et al. 1994 for more detail on TAS diagram uses.

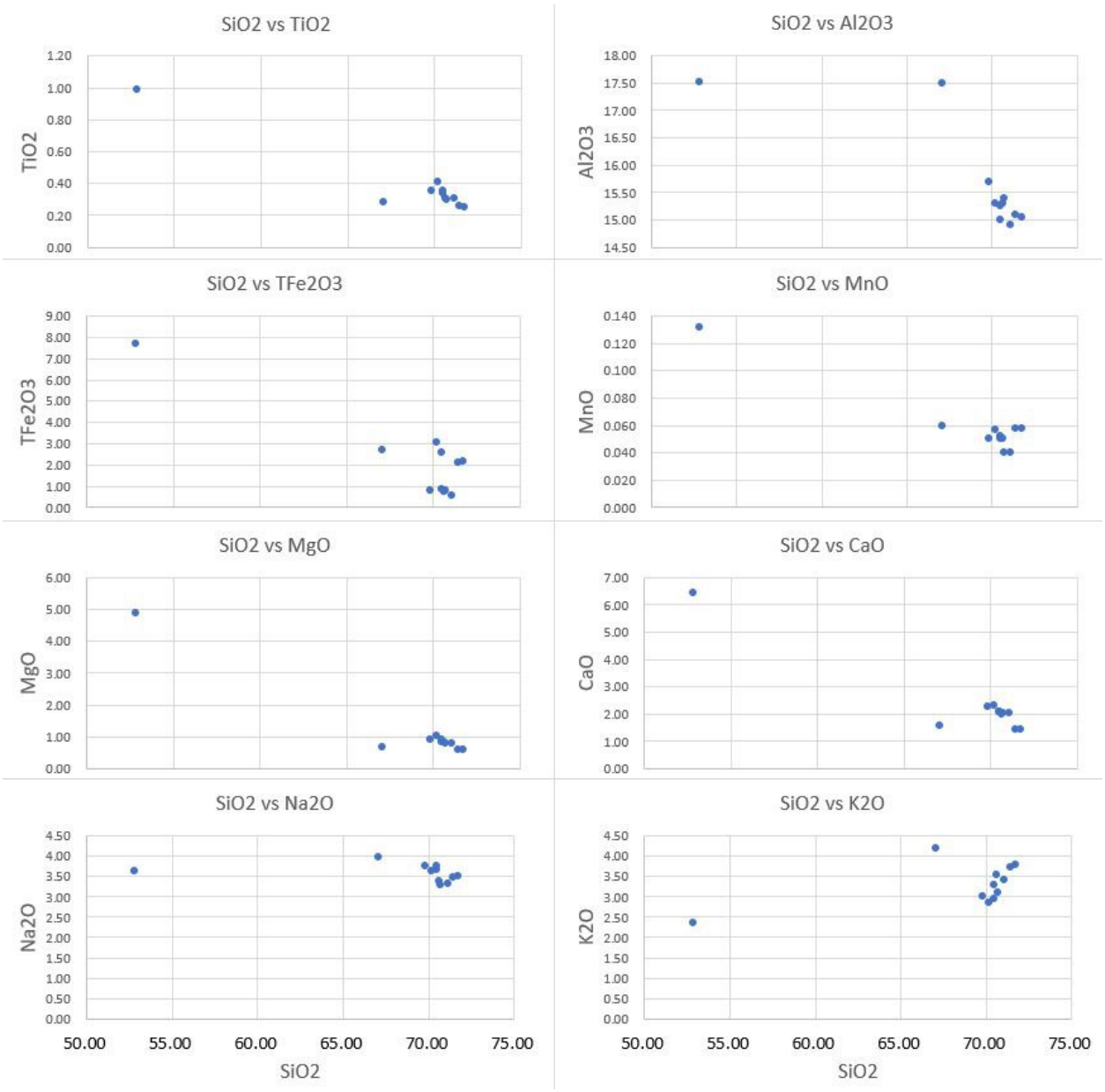

Figure 8- Harker Diagram comparing major element weight percent relative to the respective SiO_2 weight percent. Data includes samples from Stowell et al. (2019) and Foord and Cook (1989). Exact data is provided below.

Table 1- Major element data of our samples. The comparative data from Stowell et al. (2019) and Foord and Cook (1989)'s are provided in red text.

Major Elements (mass%)	21RKF1	21RKF2	21RKF3	20ROCK1	20ROCK1	10ROCK1 (Stowell)	163 (Foord)	179 (Foord)	197 (Foord)	206 (Foord)	210.5 (Foord)
SiO_2	52.84	70.2	70.48	71.73	71.4	67.06	71.1	70.7	69.8	70.5	70.6
TiO_2	0.99	0.41	0.34	0.25	0.26	0.28	0.31	0.3	0.35	0.35	0.31
Al_2O_3	17.52	15.31	15.26	15.05	15.1	17.49	14.9	15.4	15.7	15	15.3
TFe_2O_3	7.7	3.03	2.56	2.14	2.12	2.72	0.57	0.8	0.81	0.83	0.76
MnO	0.132	0.057	0.052	0.058	0.058	0.06	0.04	0.04	0.05	0.05	0.05
MgO	4.87	1.03	0.83	0.62	0.6	0.67	0.81	0.8	0.92	0.93	0.84
CaO	6.41	2.34	2.07	1.44	1.43	1.58	2.04	2.06	2.28	2.07	2.01
Na_2O	3.64	3.64	3.65	3.52	3.48	3.97	3.32	3.3	3.75	3.77	3.39
K_2O	2.36	2.87	3.28	3.8	3.71	4.21	3.43	3.09	3.01	2.95	3.54
P_2O_5	0.36	0.15	0.15	0.17	0.17	0.12	0.14	0.15	0.16	0.16	0.17
LOI	2.4	0.93	1.04	1.17	1.16	--	--	--	--	--	--
SUM	99.22	99.95	99.71	99.95	99.49	98.17	99.32	99.31	99.63	99.51	99.57

Additionally, based on major element data, the Rockford granitic samples have aluminum saturation index greater than 1.10 (Fig.9) and are peraluminous granites. Although sample 21RKF1 is not granite and is plotted below for references.

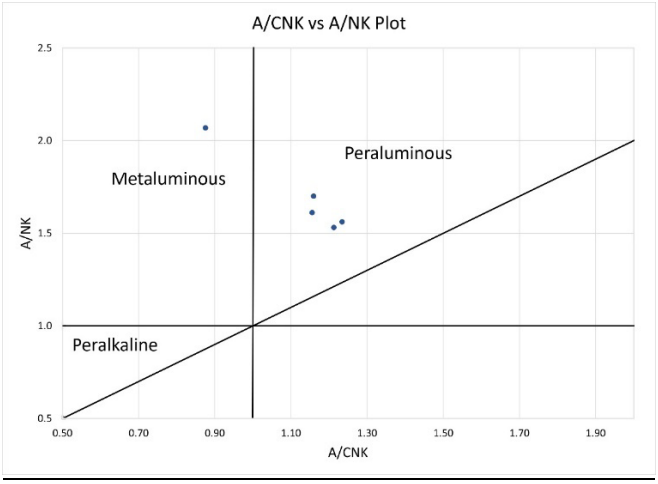

Figure 9- Modified plot from Sun et al. (2015) indicating all samples are within the peraluminous range except 21RKF1. See Sun et al. (2015) for more details. A/NK= Al/(Na+K) (molar ratios), A/CNK=Al/(Ca+Na+K) (molar ratios).

Trace and Rare Earth Element (REE) Results

All samples have chondrite-normalized light rare-earth elements (LREE)-enriched patterns and flat heavy rare-earth element (HREE) distributions. Samples 21RKF1 and 21RKF2 do not have negative Eu anomalies, suggesting the lack of fractional crystallizations for these 2 samples. In comparison, samples 21RKF3 and 20ROCK1 display minor negative Eu anomalies, indicating moderate fractional crystallization of plagioclases for these 2 samples.

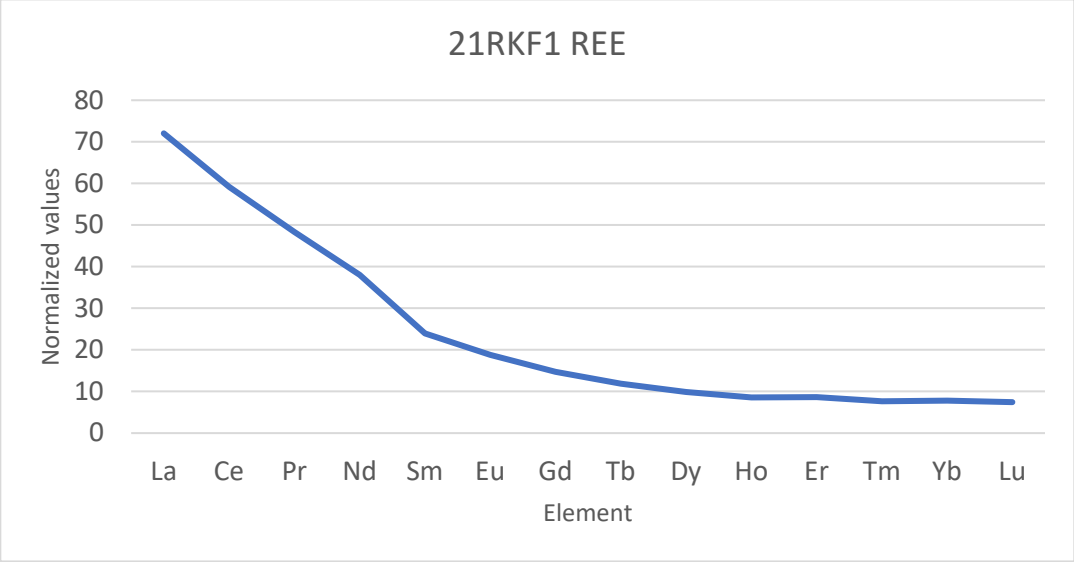

Figure 10- Chondrite-normalized rare earth element (REE) pattern for 21RKF1

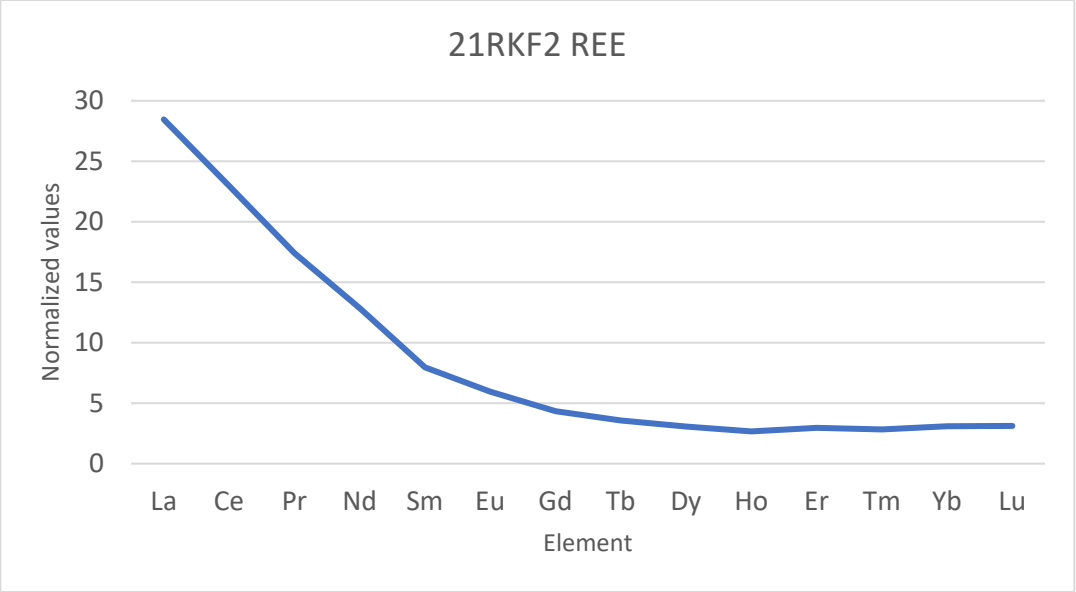

Figure 11- Chondrite-normalized REE pattern for 21RKF2

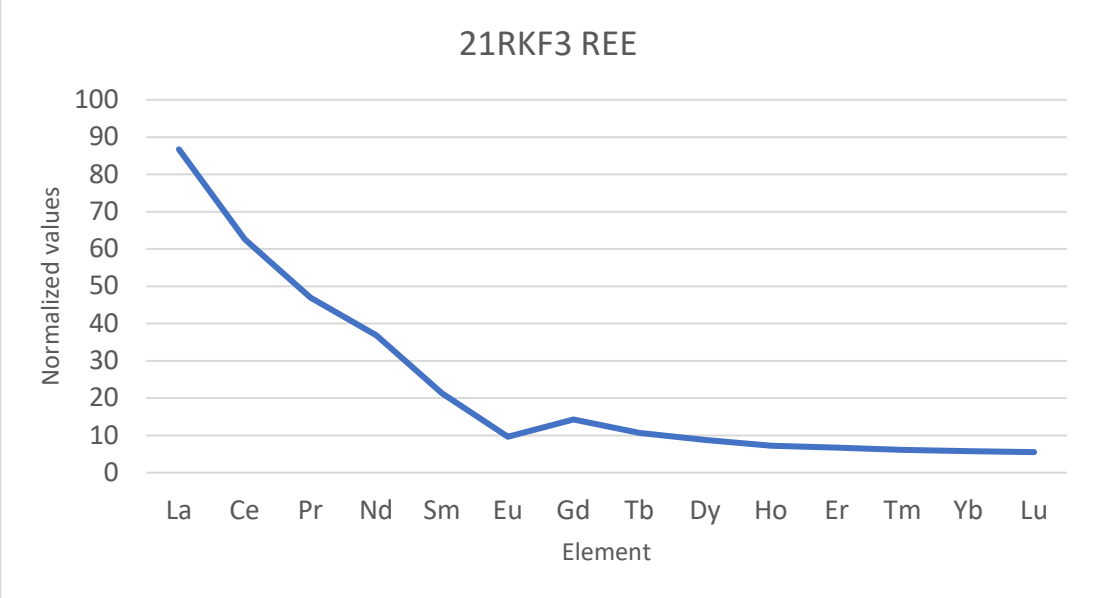

Figure 12- Chondrite-normalized REE pattern for 21RKF3

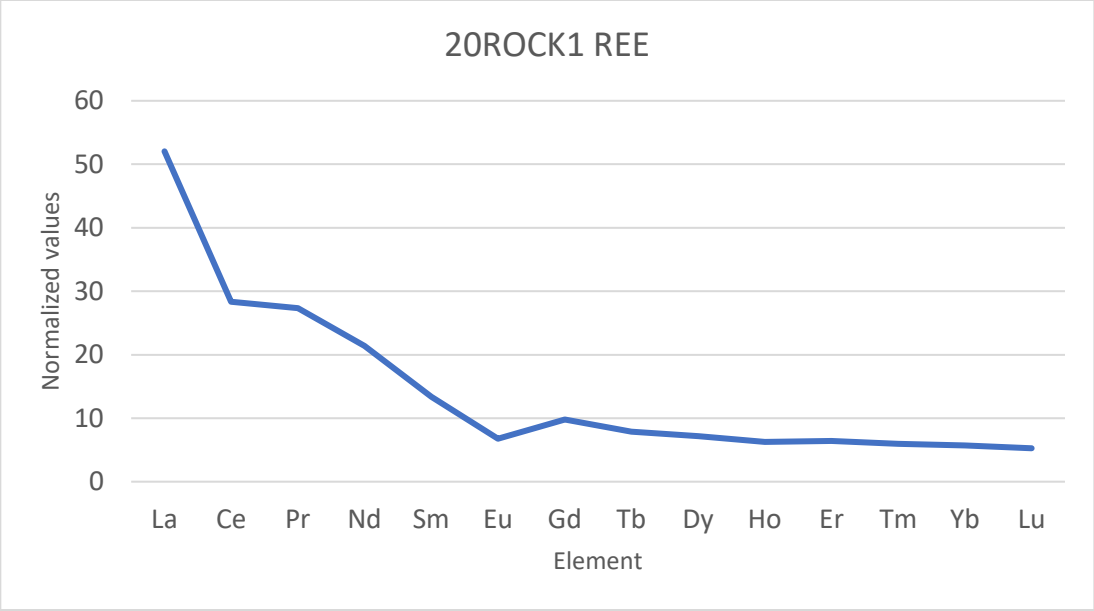

Figure 13- Chondrite-normalized REE pattern in 20ROCK1

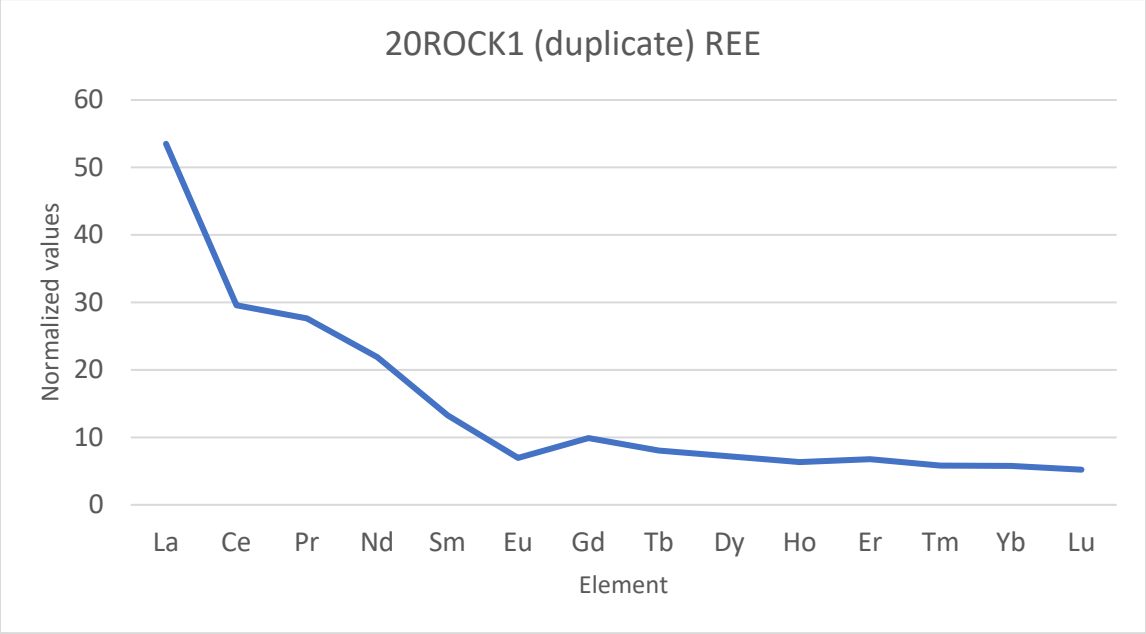

Figure 14- Chondrite-normalized REE pattern in for 20ROCK1 (duplicate)

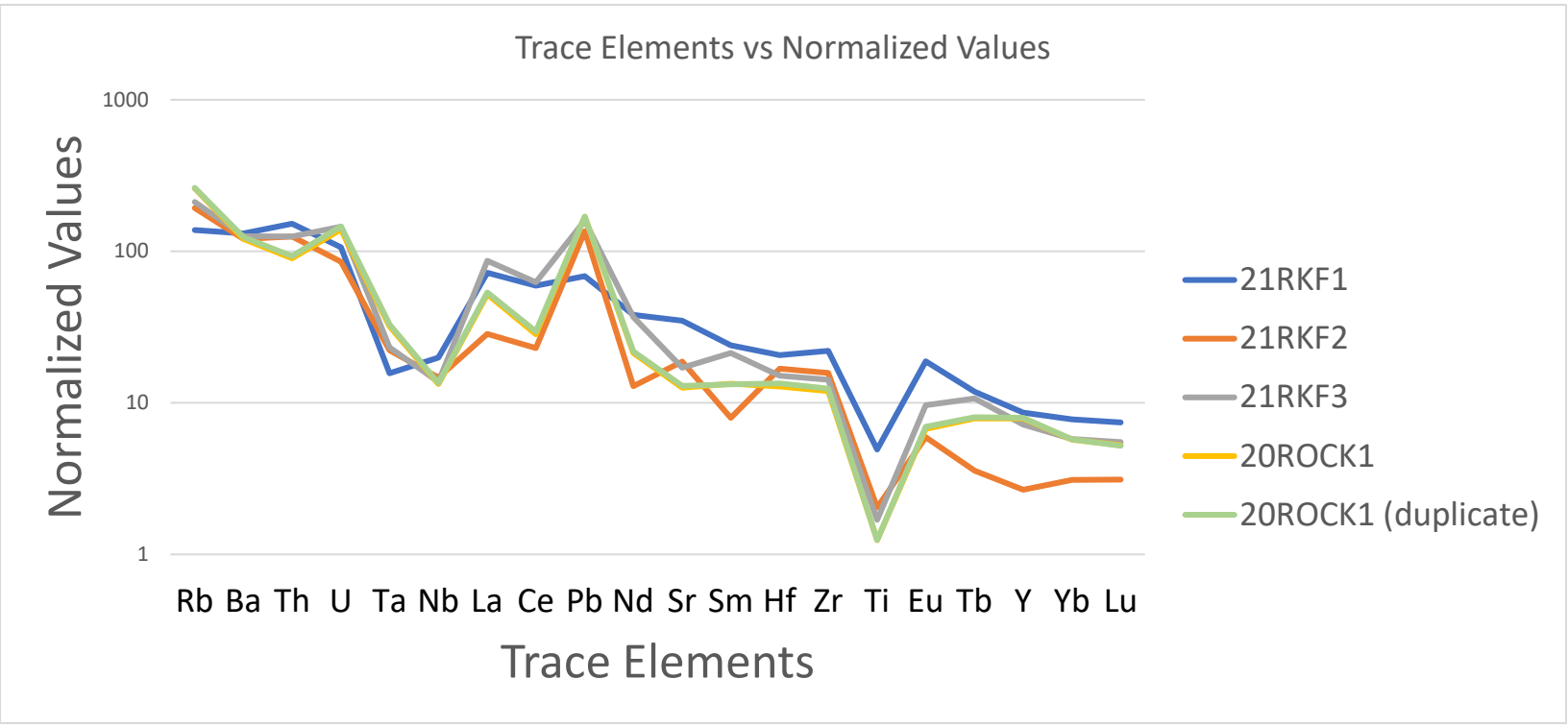

Figure 15- Primitive mantle normalized multi-element diagrams for the Rockford granite.

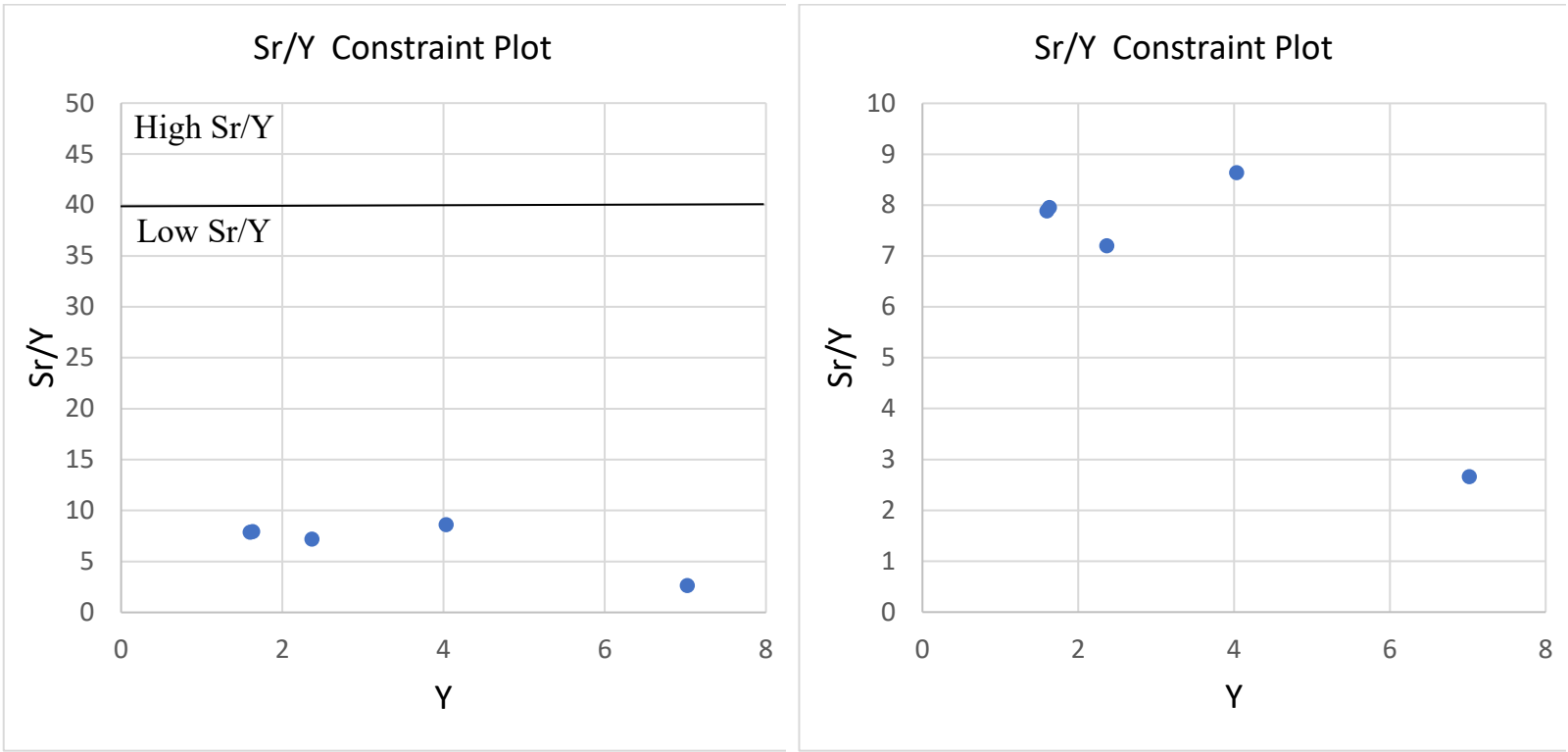

Figure 16- Sr/Y versus Y plot constraining Rockford as a low-Sr/Y magmatic body.

$^{87}Sr/^{86}Sr$ Results

The $^{87}Sr/^{86}Sr$ whole rock isotopic compositions of 4 samples (21RKF1, 21RKF2, 21RKF3, and 20ROCK1) were measured at Sample Solution Analytical Tech using an MC-ICP-MS. The $^{87}Sr/^{86}Sr$ data for all Rockford granite samples are reported in Table 2 and their respective epsilon Sr values. The calculated two-sigma error is also shown in Table 2, within the acceptable modern standard range.

Diorite sample 21RKF1 has the lowest present-day $^{87}Sr/^{86}Sr$ at 0.7065. Its age-corrected initial $^{87}Sr/^{86}Sr$ is 0.7045. Granodiorite and granite samples (21RKF2, 21RKF3, 20ROCK1) have high present-day $^{87}Sr/^{86}Sr$ vales ranging from 0.71095 to 0.71477. Their initial $^{87}Sr/^{86}Sr$ values range from 0.70477 to 0.70594. Initial epsilon Sr values are 7.0 for diorite sample 21RKF1 and from 10.4 to 27.0 for granite-granodiorite samples (21RKF2, 21RKF3, 20ROCK1).

Table 2- Whole-rock Rb, Sr concentrations and $^{87}Sr/^{86}Sr$ isotope ratios for our samples 21RKF1 and its duplicate, 21RKF2, 21RKF3, and 20ROCK1.

Sample	**Rb ppm**	**Sr ppm**	**Calculated $^{87}Rb/^{86}Sr$**	**Measured $^{87}Sr/^{86}Sr$**	**Error (2σ)**	**Initial $^{87}Sr/^{86}Sr$**	**Initial ε_{Sr}**
21RKF1	82.7	693	0.34542	0.706455	9E-06	0.704537	7.0
21RKF1 (Duplicate)	82.7	693	0.34542	0.706472	8E-06	0.704554	7.3
21RKF2	116	372	0.90298	0.710953	6E-06	0.705938	27.0
21RKF3	127	339	1.08491	0.71154	6E-06	0.705515	20.9

20ROCK1	156	251	1.80043	0.71477	6E-06	0.704772	10.4

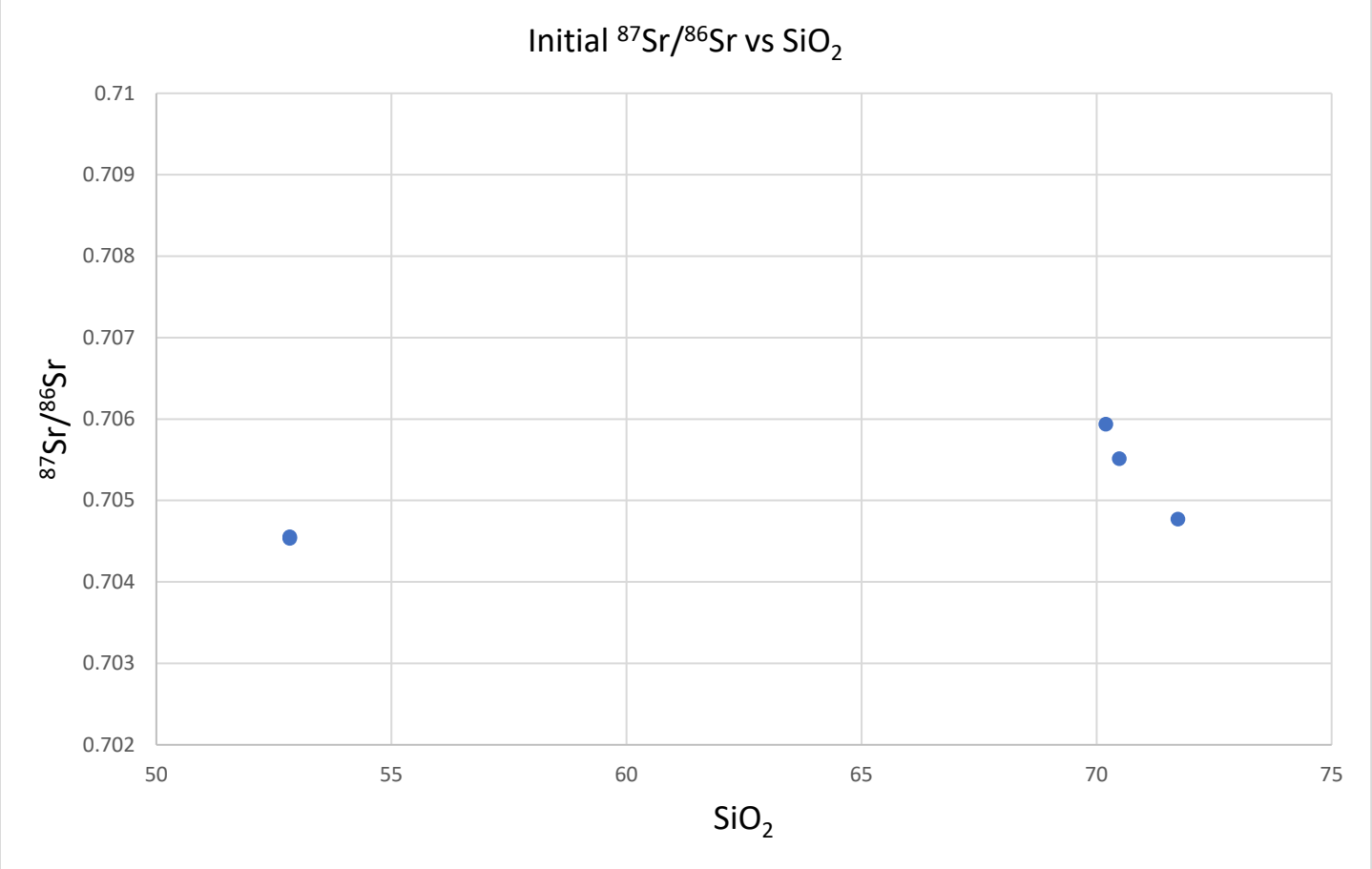

Figure 17- The $^{87}Sr/^{86}Sr$ values compared to SiO_2. Sample 21RKF1 and its duplicate $^{87}Sr/^{86}Sr$ values are 0.704537 and 0.704554, respectively. Sample 21RKF1 and its' duplicate have drastically different SiO_2 values and isotopic ratios than the rest of our samples.

$^{143}Nd/^{144}Nd$ Results

The $^{143}Nd/^{144}Nd$ whole rock isotopic compositions of 4 samples (21RKF1, 21RKF2, 21RKF3, and 20ROCK1) were measured at Sample Solution Analytical Tech using a MC-ICP-MS. The $^{143}Nd/^{144}Nd$ data followed the same protocol for all Rockford granite samples and their Sr calculated counterparts. All data is reported in Table 3 and their respective epsilon Nd values. Calculations to determine $^{147}Sm/^{144}Nd$ atomic ratio was done by multiplying the Sm/Nd ppm ratio by 0.602. The calculated two-sigma error is also shown in Table 3, which is less than Sr, but still within the acceptable modern standard range.

Diorite sample 21RKF1 has the highest present-day $^{143}Nd/^{144}Nd$ at 0.51252. Its age-corrected $^{143}Nd/^{144}Nd$ is 0.51221. The granodiorite-granite samples (21RKF2, 21RKF3, 20ROCK1) have the present-day $^{143}Nd/^{144}Nd$ values ranging from 0.51235 to 0.51239. Their age-corrected $^{143}Nd/^{144}Nd$ values range from 0.51235 to 0.51239. Diorite 21RKF1 and its duplicate have positive εNd at 1.4 to 1.5. In comparison, the granite-granodiorite samples (21RKF2, 21RKF3, 20ROCK1) have slightly negative εNd ranging from –1.8 to -1.0.

Table 3- Whole-rock Sm-Nd concentrations and $^{143}Nd/^{144}Nd$ isotope ratios for samples 21RKF1 and its duplicate, 21RKF2, 21RKF3, and 20ROCK1.

Sample	**Sm ppm**	**Nd ppm**	**Calculated $^{147}Sm/^{144}Nd$**	**Measured $^{143}Nd/^{144}Nd$**	**Error (2σ)**	**Initial $^{143}Nd/^{144}Nd$**	**ε_{Nd}**
21RKF1	9.73	47.6	0.12306	0.512524	5E-06	0.512211	1.4

21RKF1 (Duplicate)	9.73	47.6	0.12306	0.512528	4E-06	0.512215	1.5
21RKF2	3.23	16.1	0.12077	0.512350	5E-06	0.512042	-1.8
21RKF3	8.65	46	0.11320	0.512372	4E-06	0.512084	-1.0
20ROCK1	5.44	26.7	0.12265	0.512385	6E-06	0.512073	-1.3

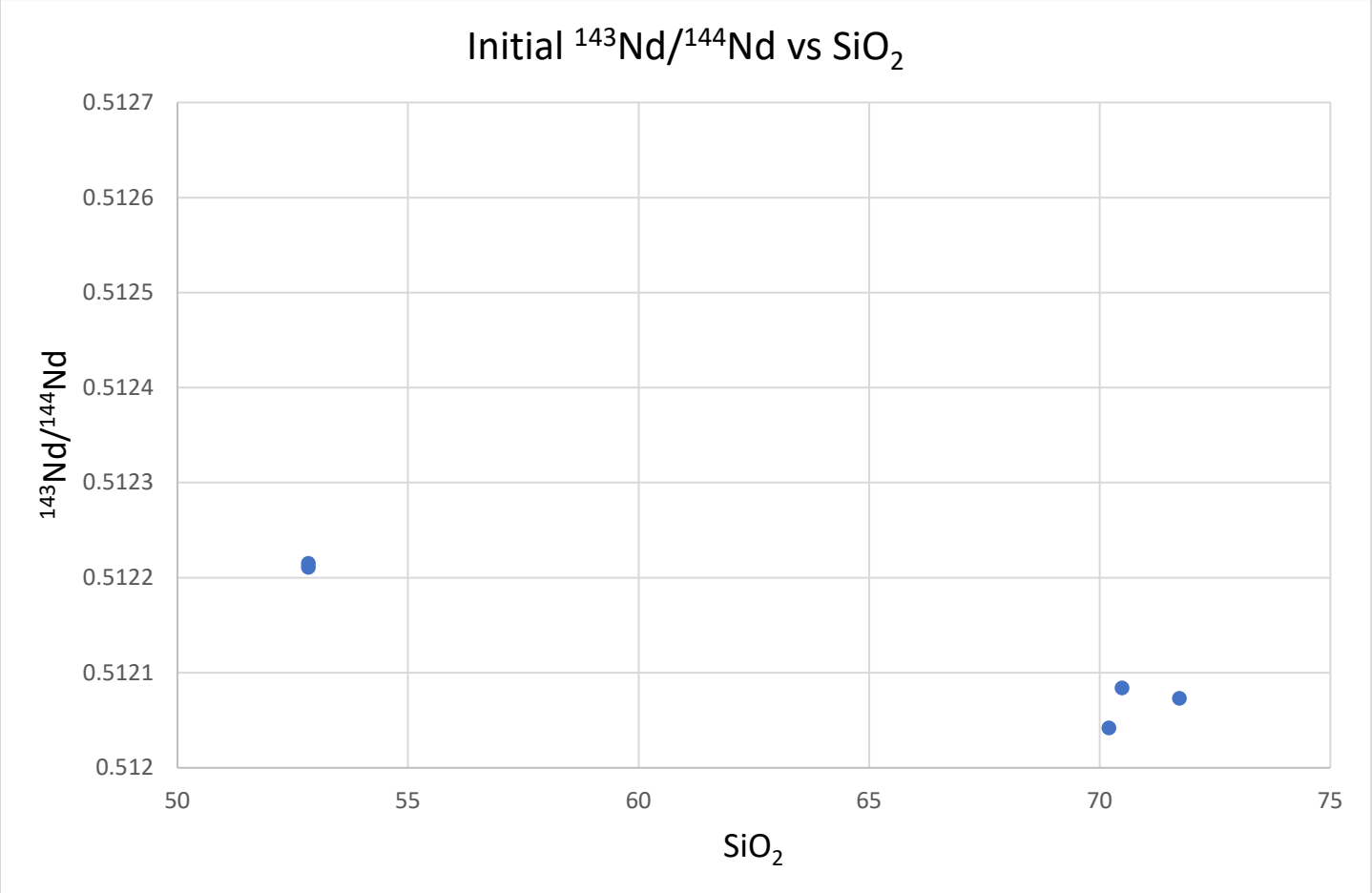

Figure 18- The $^{143}Nd/^{144}Nd$ values compared to SiO_2. 21RKF1 and its duplicate

$^{143}Nd/^{144}Nd$ values are 0.512211 and 0.512215, respectively. 21RKF1 has drastically different SiO_2 values and isotopic ratios than the rest of our samples.

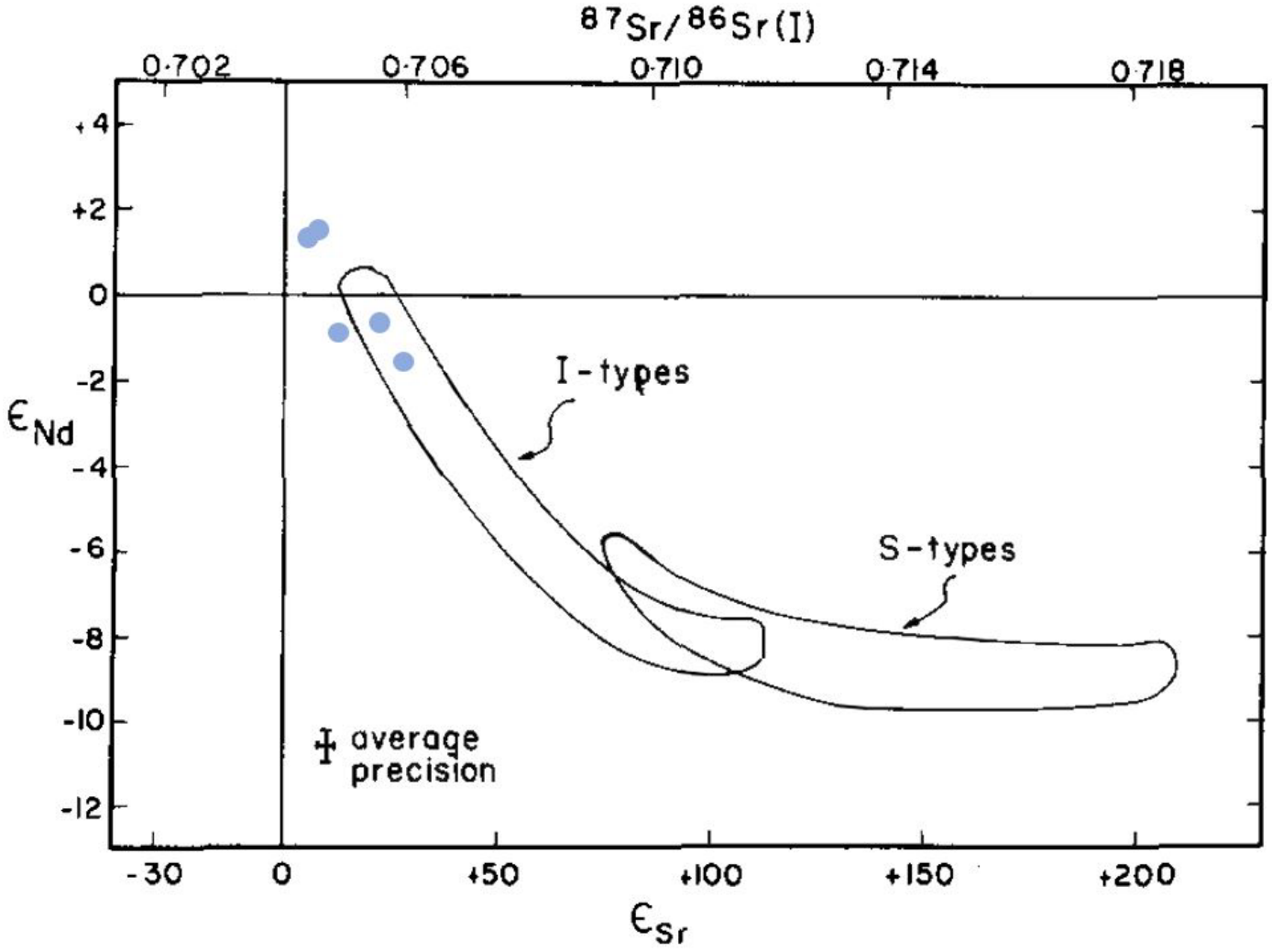

Figure 19- Modified ε_{Nd} vs ε_{Sr} chart from McCulloch and Chappell (1982) constraining primarily igneous sources for all samples, with 21RKF1 being located outside the I-type plot and at the depleted mantle source. All granitic samples from Rockford plot in the I-type granite field.

Electron Microprobe

Several point analyses were run for all samples, including the outlier sample 21RKF1. Focus was given to 21RKF1 and 21RKF3 for their distinct differences in composition and 21RKF3 is compositionally similar to 21RKF2 and 20ROCK1. All values are expected biotite oxide weight percent, with 21RKF1 having an FeO range of 14.82-16.13 and an MgO range of 12.14-13.06. 21RKF3 varies drastically having FeO and MgO values as 22.2-32.39% and 2.58-7.95% respectively.

Table 4 – Oxide Weight Percent data of biotites from Rockford collected from EMPA at Auburn University.

Sample name	SiO2	TiO2	Al2O3	FeO	MnO	MgO	CaO	Na2O	K2O	Total
21RKF1	37.75	1.99	16.25	15.57	0.2277	12.63	0.02	0.2126	9.78	94.42
21RKF1	37.67	2.13	16.27	16.13	0.2069	12.54	0.0139	0.2136	9.67	94.83
21RKF1	38.26	1.83	16.25	15.8	0.1656	12.82	0.0416	0.1563	9.78	95.1
21RKF1	37.85	2.25	16.25	16.05	0.2344	12.31	0.0521	0.0792	9.3	94.38
21RKF1	37.39	2.06	16.26	15.45	0.2358	12.76	0.035	0.2023	9.74	94.15
21RKF1	37.55	2.19	16.27	15.73	0.1742	13.06	0.0324	0.0088	9.71	94.72
21RKF2	36.37	2.72	18.41	22.06	0.6128	8.93	0.0257	N.D.	9.28	98.4
21RKF2	36.16	2.76	18.5	21.73	0.485	9.05	0.0243	0.1144	9.18	98
21RKF2	35.87	2.78	18.43	21.43	0.4866	8.65	0.0489	0.4466	9.35	97.5
21RKF2	36.18	2.87	18.26	21.51	0.6582	8.75	0.0109	0.2522	9.05	97.54
21RKF2	36.32	2.89	18.36	21.64	0.5629	9.01	0.0558	0.4062	8.47	97.71
21RKF2	35.86	2.78	18.27	22.06	0.566	8.83	0.035	0.0776	9.38	97.85
21RKF2	36.6	2.92	17.85	22.19	0.5391	8.82	0.025	0.1821	9.14	98.27
21RKF2	36.14	2.50	18.04	22.09	0.5878	9.12	N.D.	0.0258	9.21	97.71

21RKF2	35.99	2.64	18.53	22.55	0.6428	8.9	0.0202	0.0104	9.32	98.6
21RKF2	35.87	2.75	18.58	21.83	0.5787	8.84	0.0303	0.0878	9.14	97.72
21RKF2	35.15	2.70	18.57	22.51	0.5892	8.64	0.0132	0.1038	9.24	97.52
21RKF2	35.75	2.74	18.14	22.93	0.6382	8.55	0.0202	N.D.	9.37	98.14
21RKF2	34.92	2.62	18.59	22.97	0.5682	8.73	0.0195	0.0733	9.46	97.97
21RKF2	36.5	2.70	18.72	22.38	0.5831	8.39	0.0567	0.1761	9.18	98.69
21RKF2	35.26	2.73	19.12	22.63	0.5979	8.43	0.0016	N.D.	9.45	98.23
21RKF3	35.91	2.9045	16.63	22.81	0.4401	8.01	0.0126	0.0056	10	96.73
21RKF3	36.11	3.05	16.36	22.26	0.5052	7.99	0.0019	N.D.	10.12	96.4
21RKF3	35.63	2.9775	15.61	22.93	0.4063	7.95	0.0386	0.1728	10.17	95.88
21RKF3	35.16	3.05	15.81	22.85	0.4966	8	0.0696	N.D.	10.1	95.54
21RKF3	35.62	2.8708	16.52	22.97	0.5104	7.67	N.D.	0.0167	10.06	96.24
21RKF3	35.62	2.8708	16.52	22.97	0.5104	7.67	N.D.	0.0167	10.06	96.24
21RKF3	35.93	2.9049	16.41	22.98	0.502	7.85	0.0194	N.D.	10.22	96.8
21RKF3	35.52	2.8959	16.54	23.05	0.5057	7.87	0.0233	0.1176	10.27	96.81
21RKF3	35.77	2.8941	16.18	23.03	0.4614	8.07	0.0415	0.0891	9.87	96.4
21RKF3	35.41	2.9131	16.19	22.9	0.4568	7.83	N.D.	N.D.	10.08	95.78
21RKF3	35.31	2.9595	16.31	22.26	0.5125	8.05	0.0106	0.0222	10.09	95.53
21RKF3	35.45	2.9622	16.1	22.61	0.4574	8.16	0.0019	0.0613	10.11	95.92
21RKF3	35.54	2.9423	16.16	22.64	0.4385	7.92	0.0251	0.1559	10.04	95.86
21RKF3	35.63	2.8329	16.09	22.98	0.4553	8.14	0.0397	N.D.	10	96.18
21RKF3	36.25	2.9613	15.82	22.35	0.5222	7.9	0.0019	0.0614	10.34	96.21
21RKF3	35.48	2.9079	14.85	21.9	0.4775	8.01	0.0266	0.1585	10.2	94.01
21RKF3	35.79	2.7432	13.83	22.07	0.4983	7.43	0.0254	0.0847	10.34	92.81
21RKF3	35.12	2.9171	15.03	22.61	0.4772	8.05	0.0275	N.D.	10.36	94.59
20ROCK1	34.59	2.64	19.01	22.9	0.8144	7.65	N.D.	0.1998	9.17	96.97
20ROCK1	35.76	2.58	18.6	23.57	0.7622	7.66	N.D.	0.0736	9.22	98.23
20ROCK1	35.11	2.56	18.86	24.3	0.9606	7.07	0.0132	N.D.	9.22	98.1
20ROCK1	35.71	2.56	18.86	23.46	0.8683	7.27	0.0047	0.1262	9.23	98.09
20ROCK1	36.9	2.63	17.54	23.28	0.892	7.59	N.D.	N.D.	9.29	98.12
20ROCK1	36.02	2.73	17.89	23.15	0.8776	7.93	N.D.	N.D.	8.73	97.34
20ROCK1	35.95	2.65	18.33	23.56	0.8582	7.73	0.0385	N.D.	8.45	97.57
20ROCK1	35.36	2.65	17.87	23.66	0.7884	7.88	0.0047	0.058	8.24	96.51
20ROCK1	35	2.58	17.85	23.71	0.8424	7.83	0.0077	N.D.	7.97	95.79
20ROCK1	35.04	2.67	17.99	23.5	0.8298	7.82	0.0203	N.D.	9.29	97.15
20ROCK1	36.51	2.66	18.12	23.57	0.8226	7.82	0.0079	0.069	9.23	98.81
20ROCK1	35.27	2.54	18.24	23.54	0.8423	7.83	0.0148	0.1002	9.31	97.69
20ROCK1	35.6	2.69	18.81	23.7	0.7664	7.61	0.0165	N.D.	9.18	98.36
20ROCK1	36	2.49	18.39	23.03	0.809	7.83	0.0179	0.021	8.87	97.45
20ROCK1	35.93	2.53	17.85	23.07	0.8914	7.52	0.0257	N.D.	8.95	96.76
20ROCK1	36.12	2.52	18.24	23.31	0.8947	7.7	0.0148	0.0948	8.66	97.55

20ROCK1	36.39	2.63	18.23	22.82	0.8842	7.92	0.0376	0.1316	8.64	97.68
20ROCK1	36.98	2.45	18.89	22.14	0.8301	7.63	0.0507	0.0834	8.38	97.43
20ROCK1	37.91	2.58	18.71	22.52	0.9781	7.6	0.0289	N.D.	8.29	98.61
20ROCK1	36.35	2.80	18.62	23.61	0.9338	7.35	0.007	0.0633	8.87	98.6
20ROCK1	36.76	2.86	18.36	23.99	0.8738	7.25	0.0703	N.D.	8.8	98.96
20ROCK1	35.43	2.43	19.63	23.22	0.857	7.48	0.0031	0.0263	9	98.08

Discussion

Characteristics and types of the Rockford Granites

Plotting our εNd vs εSr data allowed the determination that the Rockford Granite is an I-type granite. More mafic sample 21RKF1 is plotted in the depleted mantle source. Using molar ratios in Figure 9, we determined that the Rockford Granite is peraluminous. Whereas our major element data generally is consistent with Foord (1989) and Stowell (2019), Stowell's sample is described as a quartz monzonite in the TAS diagram (Figure 7). Foord's (1989) data corresponds well with our granodiorite identification and indicates reproducibility in our data.

Tectonic setting and the role of mantle contributions

Selected trace element discrimination diagrams can be used to infer ancient tectonic setting for granites (Pearce et al., 1985) and have been widely used in the study of granitic rocks (e.g., Ozdamar et al., 2021). The Rockford granites consistently plot in the VAG (volcanic arc granite) field in granite discrimination diagrams (Figure 19).

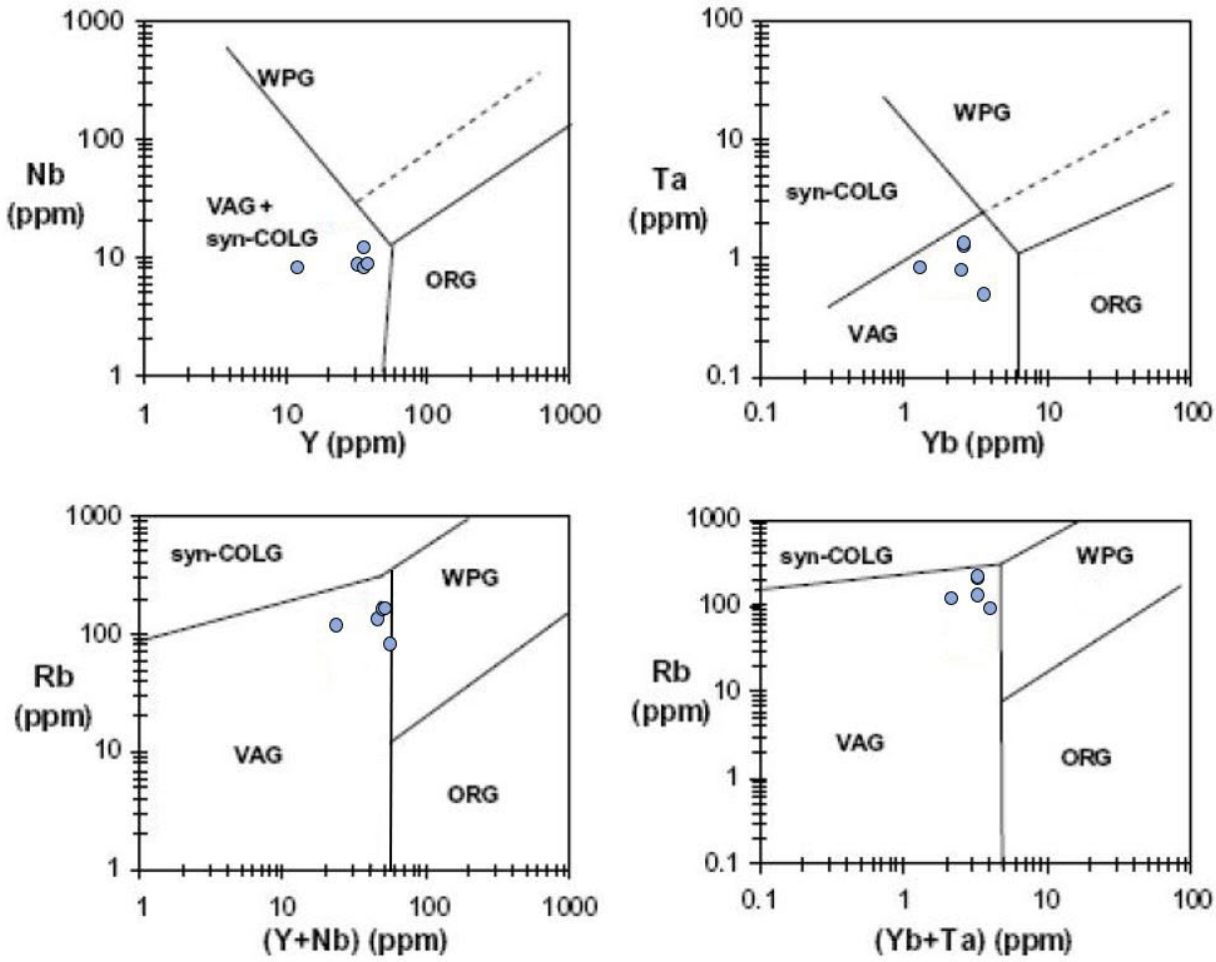

Figure 20- Modified Pearce et al. (1984) granite discrimination diagrams for samples in this study. Exact data provided in Table A-3 in the Appendix section. VAG= volcanic arc granite, WPG= within plate granite, Syn-COLG= syn-tectonic collision granite, ORG= ocean ridge granite.

Diorite sample 21RKF1 plot in the depleted mantle domain in Sr vs Nd isotope diagram and may approach the isotopic compositions of mantle end member. Granitic samples 21RKF2, 21RKF3, and 20ROCK1 have relatively high εNd and low εSr relative to S-type granites and plot in the I-type granite field. The Sr-Nd isotope plot suggests significant mantle material

contributions to the genesis of the Rockford granites.

Magma temperature and oxygen fugacity conditions

Temperatures calculated from biotite data calculated from the EMPA range from 618 to 652 °C. The geothermometer calculation formula from Luhr et al. 1984 is:

$T(°C) = 838/(1.0337-Ti/Fe^{2+})-273$.

Biotite chemistry collected from the EMPA was processed and placed onto a constraint diagram modified from Anderson (2008). Biotites from granitic samples yield oxygen fugacity of ΔQFM+1.0. Note that highly reducing magmas in a rift setting may have oxygen fugacity as low as ΔQFM-2.0 (Zou et al., 2021). Rockford granites formed in a relatively oxidizing environment. Arc magmas may have oxygen fugacity values ranging from ΔQFM0.0 to ΔQFM+4.0. The Rockford granites with ΔQFM+1.0 formed in an arc environment.

If this biotite diagram also works for diorite, then the diorite sample (21RKF1) formed in a more oxidizing environment (ΔQFM+2.3) than the granitic samples (21RKF2, 21RKF3, 20ROCK1).

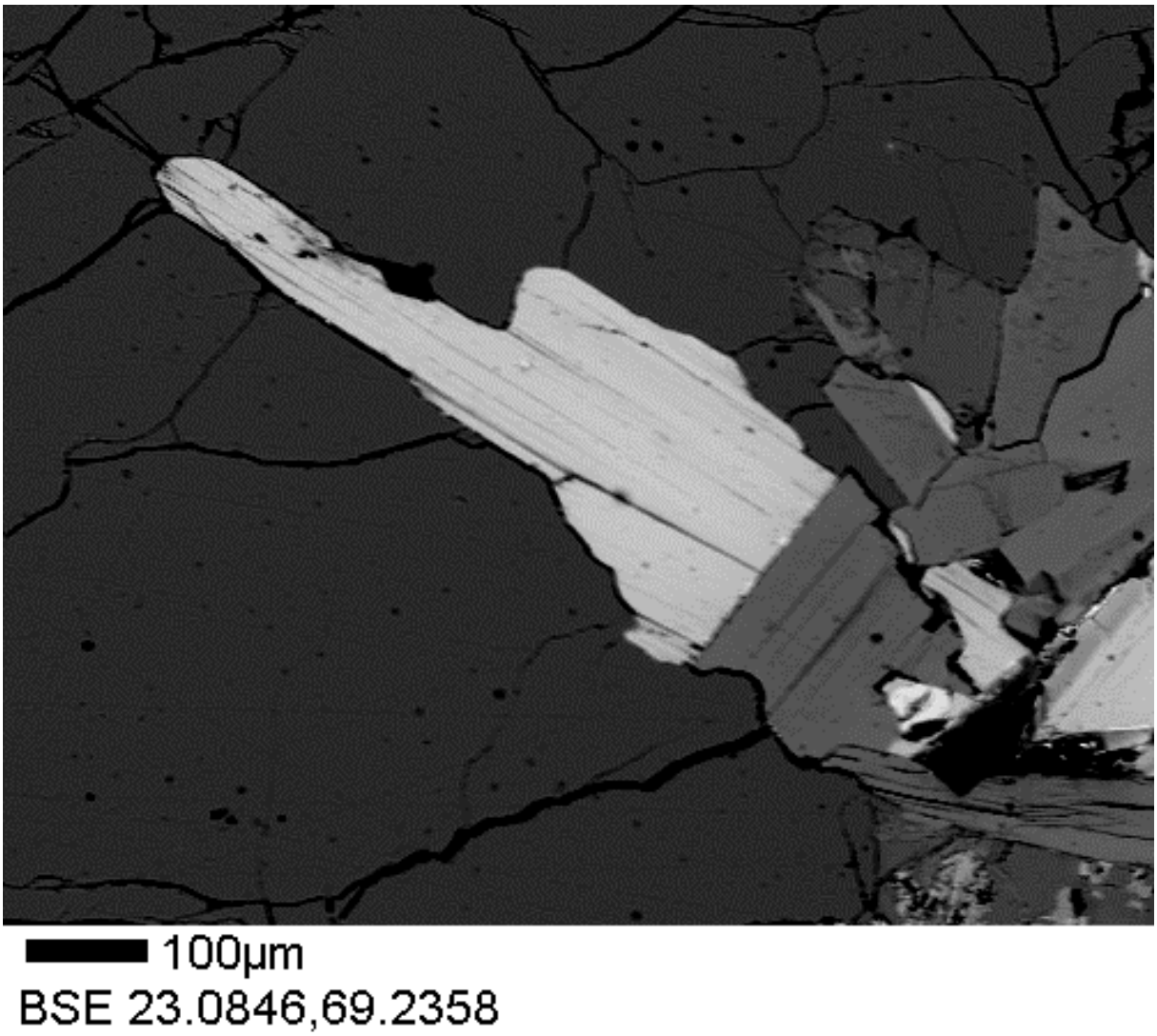

Figure 21- BSE image of a biotite grain in sample 21RKF3 captured on the AU-EMPA.

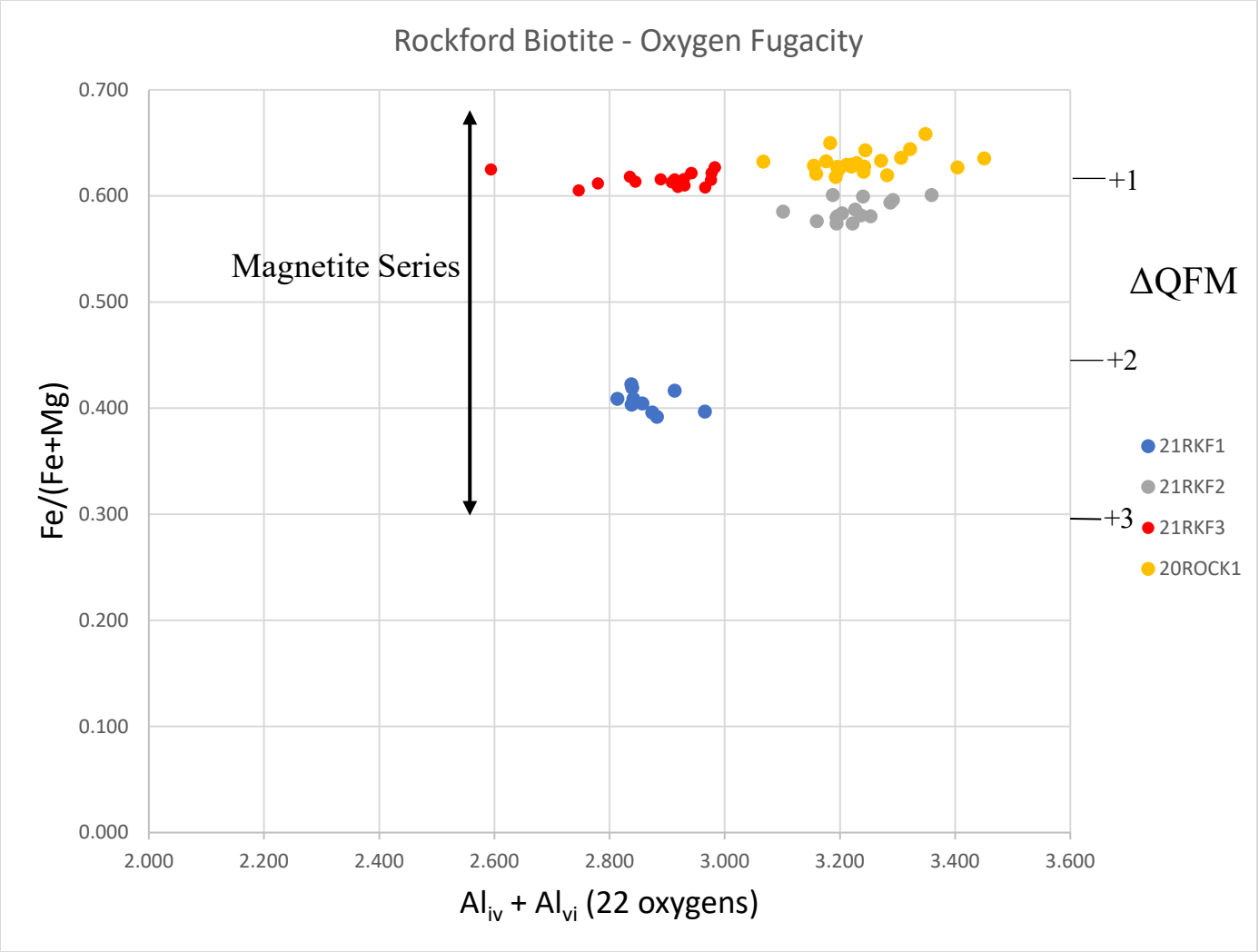

Figure 22- Modified constraint diagram from Anderson (2008). Data is calculated from the Fe/(Fe+Mg) ratio versus Al_{iv} + Al_{vi}. QFM- Quartz-Fayalite-Magnetite buffer.

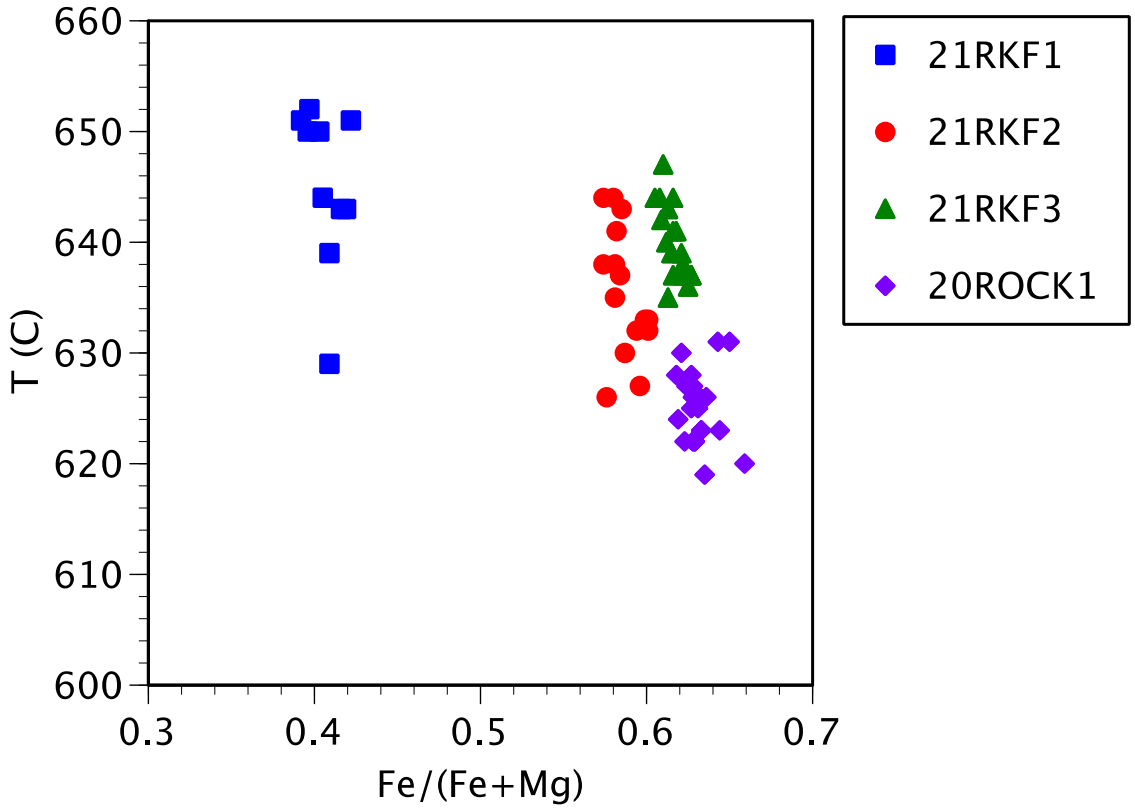

Figure 23- Temperature constraint diagram using methods from Luhr et al. (1984). All temperature values were obtained in Kelvin and then converted to Celsius.

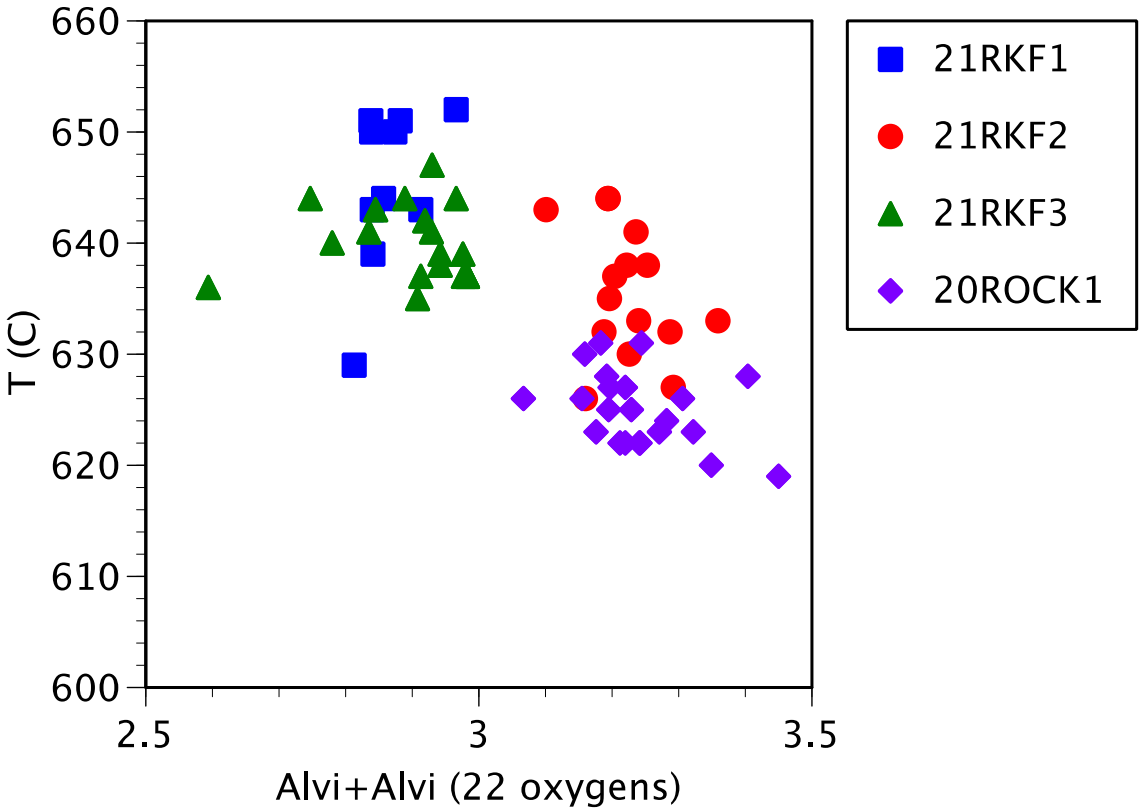

Figure 24- Temperature constraint diagram using methods from Luhr et al. (1984). All temperature values were obtained in Kelvin and then converted to Celsius.

Conclusions

1. The granites within the Rockford Granite have relatively low initial ε_{Sr} and high initial ε_{Nd}. further, they are peraluminous granites; and they have low Sr/Y ratios. Trace element discrimination diagram indicates that the Rockford Granite belongs volcanic arc granites.

2. The high initial ε_{Nd} values of the Rockford's granites and granodiorites (-1.0 to -1.8), and the plot of ε_{Sr} versus ε_{Nd}, indicate that these granites are I-type. In I-type granites, the mantle not only contributed heat for crustal partial melting, but also contributed juvenile mantle materials.

3. The Rockford granites were formed at temperatures ranging from approximately 618-652°C, and oxidizing oxygen fugacity conditions of ΔQFM+1.0, consistent with their I-type character and volcanic arc setting.

References

Anderson, Lawford J., Barth, Andrew P., Frank Mazdab, Joseph L.W., 2008. Thermometers and Thermobarometers in Granitic Systems. Reviews in Mineralogy & Geochemistry 69, 121-142.

Copeland, Charles W., Beg, Mirza A., 1979. Geology of the Birmingham, Gadsden, and Montgomery 1° x 2° NTMS Quadrangles, Alabama. Geological Survey of Alabama.

Doroozi, R., et al., 2015. Cretaceous alkaline volcanism in south Marzanabad, northern central Alborz, Iran: Geochemistry and petrogenesis. Geoscience Frontiers 7, 11.

Drummond, M.S., Ragland, P.C., Wesolowski, D., 1986. An example of trondhjemite genesis by means of alkali metasomatism: Rockford Granite, Alabama Appalachians. Contributions to Mineralogy and Petrology 93, 98-113.

Drummond, M.S., Wesolowski, David, Allison, David T., 1988. Generation, Diversification, and Emplacement of the Rockford Granite, Alabama Appalachians: Mineralogic, Petrologic, Isotopic (C&O), and P-T Constraints. Journal of Petrology, 29-4, 869-897.

Faure, G. and Mensing, T.M., 2005. Isotopes: Principles and Applications. Third Edition. 897pp.

Foord, Eugene E., Cook, Robert B., 1989. Mineralogy and Paragenesis of the McAllister Sn-Ta Bearing Pegmatite, Coosa County, Alabama. Canadian Mineralogist 27, 93-105.

Li, C.F., Li, X.H., Li, Q.L., Guo, J.H. and Yang, Y.H., 2012. Rapid and precise determination of Sr and Nd isotopic ratios in geological samples from the same filament loading by

thermal ionization mass spectrometry employing a single-step separation scheme. Analytica Chimica Acta, 727 (10), 54–60.

Luhr, James F., Carmichael, Ian S.E., Varekamp, Johan C., 1984. The 1982 eruptions of el chichon volcano, Chiapas, Mexico: Mineralogy and petrology of the anhydrite-bearing pumices. Journal of Volcanology and Geothermal Research 23, 69-108.

Ma, C., VanDevervoort, Dane S., Steltenpohl, Mark G., Schwartz, Joshua J., 2019. Formation and Orogen-Parallel Transport of the Dadeville Complex, Alabama, USA: Implications for the Taconian Orogeny in the Southern Appalachians. American Journal of Science 319, 562-630.

McCulloch, Malcolm T., Chappell, Bruce W., 1981. Nd isotopic characteristics of S- and I-type granites. Earth and Planetary Science Letters, 58, 51-64.

McDonough W.F., Sun S.-s. 1995. The composition of the Earth. Chemical Geology 120, 223-253.

Middlemost, Eric A.K., 1994. Naming materials in the magma/igneous rock system. Earth Science Reviews 37, 215-224.

Moyen, Jean-Francois, 2009. High Sr/Y and La/Yb ratios: The meaning of the “adakitic signature.” Lithos 112, 556-574.

Özdamar, Ş., Roden, M.F., Zou, H.B., Billor, M.Z., Hames, W.E., Georgiev, S., Dunkl, I., 2021. Petrogenesis of Oligocene plutonic rocks in western Anatolia (NW Turkey): Insights

from mineral and rock chemistry, Sr-Nd isotopes, and U-Pb, Ar-Ar and (U-Th)/He geochronology. Geochemistry 81, 125747.

Patino, Alberto E., Castro Antonio, Fernandez, Carlos, Vigneresse Jean L., 1999. Understanding Granites: Integrating New and Classical Techniques. Geological Society of London 168, 55-75.

Pearce, Julian A., Harris, Nigel B.W., Tindle, Andrew G., 1984. Trace Element Discrimination Diagrams for the Tectonic Interpretation of Granitic Rocks. Journal of Petrology 25, 956-983.

Rankin, Douglas W., 1975. The Continental Margin of Eastern North America in the Southern Appalachians: The Opening and Closing of the Proto-Atlantic Ocean. American Journal of Science 275-A, 298-336.

Russell, G.S., Odom, A.L., and Russell, C.W., 1987, Uranium-lead and rubidium-strontium isotopic evidence for the age and origin of granitic rocks in the northern Alabama Piedmont, in Drummond, M.S., and Green, N.L., eds., Granites of Alabama: Tuscaloosa, Alabama Geological Survey, 239–249.

Stow, S.H., Neilson, M.J., Neathery, T.L., 1984. Petrography, Geochemistry, and Tectonic Significance of the Amphibolites of the Alabama Piedmont. American Journal of Science 284, 416-436.

Stowell, H.H., Schwartz, J.J., Ingram III, S.B., Madden, J., Jernigan, C., Steltenpohl, M., Mueller, P., 2019. Linking metamorphism, magma generation, and synorogenic

sedimentation to crustal thickening during Southern Appalachian mountain building, USA. The Geological Society of America, 722-749.

Sun, Fajun, Xu, Xisheng, Zou, Haibo, Xia, Yan, 2015. Petrogenesis and magmatic evolution of ~130 Ma A-type granites in Southeast China. Journal of Asian Earth Sciences 98, 209-224.

Tindle, Andrew G., Webb, Peter C., 1990. Estimation of lithium contents in triochtahedral micas using microprobe data: application to micas from granitic rocks. Eur. J. Mineral 2, 595-610.

U.S. Geological Survey, 2021, Mineral commodity summaries 2021: U.S. Geological Survey, 200

Wei, F., Prytulak, J., Xu, J., Wei, W., Hammond, J., Zhao, B., 2017. The cause and source ofmelting for the most recent volcanism in Tibet: A combined geochemical and geophysical perspective. Lithos 288-289: 175-190.

Zandomeni, Priscila S., Moreno, Juan A., Verdecchia, Sebastian O., 2021. Crystallization Conditions and Petrogenetic Characterization of Metaluminous to Peraluminous Calc-Alkaline Orogenic Granitoids from Mineralogical Systematics: The Case of the Cambrian Magmatism from the Sierra de Guasayan (Argentina). Minerals 11, 166.

Zeng, Lingsen, Gao, Li-E, Xie, Kejia, Zheng-Liu, Jing, 2011. Mid-Eocene high Sr/Y granites in the Northern Himalayan Gneiss Domes: Melting thickened lower

continental crust. Earth and Planetary Science Letters 303, 251-266.

Zou, Haibo, Vazquez, Jorge, Fan, Qicheng, 2020. Timescales of magmatic processes in post-collisional potassic lavas, northwestern Tibet. Lithos 358-359, 105418.

Zou, H.B., Zindler, A., Xu, X.S., Qi, Q., 2000. Major and trace element, and Nd-Sr-Pb isotope studies of Cenozoic basalts in SE China: mantle sources, regional variations, and tectonic significance. Chemical Geology 171, 33-47.

Zou, H.B., Vazquez, J., Zhao, Y.W., Guo, Z.P. (2021) Zircon surface crystallization ages for the extremely reduced magmatic products of the Millennium Eruption, Changbaishan Volcano (China/North Korea). Gondwana Research 92: 172-183.

Appendix

Table A-1

	21RKF1 sample (ppm)	21RKF2 sample (ppm)	21RKF3 sample (ppm)	20ROCK1 sample (ppm)	20ROCK1 duplicate (ppm)
Li	170	108	70.4	100	102
Be	1.69	2.59	3.31	3.78	3.80
Sc	22.5	7.42	6.85	6.02	6.06
V	165	45.2	34.0	24.4	24.7
Cr	99.2	16.3	12.4	8.21	8.43
Co	20.5	2.93	2.55	2.39	2.51
Ni	22.4	4.42	3.70	4.17	4.09
Cu	58.0	5.75	5.67	6.79	6.82
Zn	109	87.5	77.0	129	131
Ga	21.1	19.0	18.8	18.2	18.1
Rb	82.7	116	127	156	157
Sr	693	372	339	251	258
Y	37.1	11.5	31.0	33.9	34.2
Zr	231	165	149	126	131
Nb	13.1	9.68	9.05	8.76	8.89
Sn	5.40	4.03	4.39	5.94	5.85
Cs	5.08	5.50	5.97	6.85	6.98
Ba	867	794	830	796	817
La	46.7	18.4	56.2	33.7	34.7
Ce	99.2	38.5	105	47.4	49.6
Pr	12.3	4.42	11.9	6.94	7.01
Nd	47.6	16.1	46.0	26.7	27.3
Sm	9.73	3.23	8.65	5.44	5.38
Eu	2.89	0.92	1.49	1.04	1.07
Gd	8.01	2.36	7.75	5.32	5.39
Tb	1.17	0.35	1.06	0.78	0.80
Dy	6.64	2.07	5.94	4.83	4.85
Ho	1.28	0.40	1.08	0.93	0.95
Er	3.80	1.30	2.96	2.80	2.97
Tm	0.52	0.19	0.41	0.40	0.40
Yb	3.43	1.37	2.54	2.52	2.54
Lu	0.50	0.21	0.37	0.36	0.35
Hf	5.85	4.75	4.28	3.64	3.80
Ta	0.58	0.82	0.86	1.18	1.22

Tl	0.79	0.75	0.81	0.96	1.04
Pb	10.3	20.3	23.9	25.3	25.5
Th	12.1	9.94	9.96	7.15	7.39
U	2.16	1.73	2.95	2.82	2.97

Table A-2

Element normalization values (McDonough 1995, pg.238)	ppm
Li	1.6
Be	0.068
Sc	16.2
V	82
Cr	2625
Co	105
Ni	1960
Cu	30
Zn	55
Ga	4
Rb	0.6
Sr	19.9
Y	4.3
Zr	10.5
Nb	0.658
Sn	0.13
Cs	0.021
Ba	6.6
La	0.648
Ce	1.675
Pr	0.254
Nd	1.25
Sm	0.406
Eu	0.154
Gd	0.544
Tb	0.099
Dy	0.674
Ho	0.149
Er	0.438
Tm	0.068
Yb	0.441
Lu	0.0675
Hf	0.283
Ta	0.037
Tl	0.0035
Pb	0.15
Th	0.0795
U	0.0203

Table A-3

Normalized data values (sample mass/normalization value) (McDonough 1995, pg.238)					
	21RKF1 sample	21RKF2 sample	21RKF3 sample	20ROCK1 sample	20ROCK1 duplicate
Li	106.5	67.4	44.0	62.7	63.7
Be	24.8	38.1	48.6	55.5	55.9
Sc	1.4	0.5	0.4	0.4	0.4
V	2.0	0.6	0.4	0.3	0.3
Cr	0.0	0.0	0.0	0.0	0.0
Co	0.2	0.0	0.0	0.0	0.0
Ni	0.0	0.0	0.0	0.0	0.0
Cu	1.9	0.2	0.2	0.2	0.2
Zn	2.0	1.6	1.4	2.4	2.4
Ga	5.3	4.7	4.7	4.6	4.5
Rb	137.9	193.1	211.7	260.2	262.3
Sr	34.8	18.7	17.0	12.6	13.0
Y	8.6	2.7	7.2	7.9	8.0
Zr	22.0	15.7	14.2	12.0	12.4
Nb	19.9	14.7	13.8	13.3	13.5
Sn	41.6	31.0	33.8	45.7	45.0
Cs	242.1	261.7	284.2	326.4	332.4
Ba	131.4	120.4	125.8	120.7	123.9
La	72.0	28.5	86.7	52.0	53.5
Ce	59.2	23.0	62.6	28.3	29.6
Pr	48.3	17.4	47.0	27.3	27.6
Nd	38.1	12.9	36.8	21.4	21.9
Sm	24.0	8.0	21.3	13.4	13.2
Eu	18.8	5.9	9.7	6.7	7.0
Gd	14.7	4.3	14.3	9.8	9.9
Tb	11.9	3.6	10.7	7.9	8.0
Dy	9.9	3.1	8.8	7.2	7.2
Ho	8.6	2.7	7.2	6.2	6.4
Er	8.7	3.0	6.8	6.4	6.8
Tm	7.6	2.8	6.1	5.9	5.8
Yb	7.8	3.1	5.8	5.7	5.8
Lu	7.4	3.1	5.5	5.3	5.2
Hf	20.7	16.8	15.1	12.9	13.4
Ta	15.7	22.3	23.3	32.0	32.9
Tl	224.5	213.2	230.7	274.0	296.2
Pb	68.4	135.4	159.5	168.6	169.7
Th	152.1	125.0	125.3	90.0	93.0
U	106.2	85.4	145.5	139.1	146.4

Table A-4

EMPA element order	TAP/1	TAP/2	PET/3	LIF/4
Na	✓			
Mg	✓			

Al7	✓			
Si1		✓		
K			✓	
Ca5			✓	
Ti3			✓	
Mn				✓
Fe2				✓